Available online at www.sciencedirect.com

ScienceDirect

Geochimica et Cosmochimica Acta 318 (2022) 510–530

Geochimica et Cosmochimica Acta

www.elsevier.com/locate/gca

No ion is an island: Multiple ions influence boron incorporation into $CaCO_3$

Michael J. Henehan [a,b,*], Christa D. Klein Gebbinck [c], Jillian V.B. Wyman [c], Mathis P. Hain [d], James W.B. Rae [e], Bärbel Hönisch [f], Gavin L. Foster [b], Sang-Tae Kim [c]

[a] Section 3.3 Earth Surface Geochemistry, Deutsches GeoForschungsZentrum GFZ, Telegrafenberg, 14473 Potsdam, Germany
[b] School of Ocean and Earth Science, University of Southampton Waterfront Campus, National Oceanography Centre, Southampton, European Way, Southampton SO14 3ZH, Hampshire, UK
[c] School of Earth, Environment and Society, McMaster University, 1280 Main Street West, Hamilton, ON L8S 4K1, Canada
[d] Earth and Planetary Sciences Department, University of California Santa Cruz, 1156 High Street, Santa Cruz, CA 95064, USA
[e] School of Earth and Environmental Sciences, University of St Andrews, St Andrews KY16 9AL, UK
[f] Lamont-Doherty Earth Observatory of Columbia University, Palisades, NY 10964, USA

Received 18 February 2021; accepted in revised form 10 December 2021; Available online 17 December 2021

Abstract

Boron isotope ratios – as measured in marine calcium carbonate – are an established tracer of past seawater and calcifying fluid pH, and thus a powerful tool for probing marine calcifier physiology and reconstructing past atmospheric CO_2 levels. For such applications, understanding the inorganic baseline upon which foraminiferal vital effects or coral pH upregulation are superimposed should be an important prerequisite. Yet, investigations into boron isotope fractionation in synthetic $CaCO_3$ polymorphs have often reported variable and even conflicting results, implying our understanding of the pathways of boron incorporation into calcium carbonate is incomplete. Here we address this topic with experimental data from synthetic calcite and aragonite precipitated across a range of pH in the presence of both Mg and Ca. We observe coherent patterns in B/Ca and Na/Ca ratios that, we suggest, point to paired substitution of Na and B into the carbonate lattice to achieve local charge balance. In addition, we confirm the results of previous studies that the boron isotope composition of inorganic aragonite precipitates closely reflects that of aqueous borate ion, but that inorganic calcites display a higher degree of scatter, and diverge from the boron isotope composition of aqueous borate ion at low pH. With reference to the simultaneous incorporation of other trace and minor elements, we put forward possible explanations for the observed variability in the concentration and isotopic composition of boron in synthetic $CaCO_3$. In particular, we highlight the potential importance of interface electrostatics in driving variability in our own and published synthetic carbonate datasets. Importantly for palaeo-reconstruction, however, these electrostatic effects are unlikely to play as important a role during natural precipitation of biogenic carbonates.

Keywords: Boron Isotopes; Calcite; Aragonite; $\delta^{11}B$; pH proxy; Trace Element Incorporation

* Corresponding author at: Section 3.3 Earth Surface Geochemistry, Deutsches GeoForschungsZentrum GFZ, Telegrafenberg, 14473 Potsdam, Germany.

E-mail addresses: henehan@gfz-potsdam.de (M.J. Henehan), ckleingebbinck@hotmail.com (C.D. Klein Gebbinck), wymanjv@mcmaster.ca (J.V.B. Wyman), mhain@ucsc.edu (M.P. Hain), jwbr@st-andrews.ac.uk (J.W.B. Rae), hoenisch@ldeo.columbia.edu (B. Hönisch), gavin.foster@noc.soton.ac.uk (G.L. Foster), sangtae@mcmaster.ca (S.-T. Kim).

https://doi.org/10.1016/j.gca.2021.12.011
0016-7037/

1. INTRODUCTION

The boron isotope-pH proxy, as applied to fossil and modern biogenic carbonates such as foraminifera and corals, is increasingly used to reconstruct both past ocean pH and atmospheric CO_2 levels (e.g. Penman et al., 2014; Martínez-Botí et al., 2015; Anagnostou et al., 2016; Babila et al., 2018; Henehan et al., 2020) and to provide key insights into the processes controlling biomineralisation (e.g. McCulloch et al., 2012). Aside from the demonstrable ability of the proxy to reproduce past CO_2 levels recorded in ice cores (e.g. Chalk et al., 2017) and its capacity to reconstruct the carbonate chemistry of the calcifying fluid in stony corals (e.g. Holcomb et al., 2014; Gagnon et al., 2021), its widespread adoption (at least initially) was fuelled by its strong mechanistic basis, rooted in straightforward inorganic aqueous geochemistry. This mechanistic basis, and its refinement through time, is extensively detailed elsewhere (e.g. Hemming and Hanson, 1992; Foster and Rae, 2016; Rae, 2018; Hönisch et al., 2019), but can be briefly summarised as follows: (i) boron dissolved in seawater speciates primarily between tetrahydroxyborate, or borate ion ($B(OH)_4^-$), and boric acid ($B(OH)_3$) according to ambient pH, (ii) there is a well-defined boron isotope fractionation associated with this speciation, (iii) the charged borate ion is predominantly incorporated into the $CaCO_3$ crystal structure without isotopic fractionation, and thus (iv) the isotopic composition (and perhaps concentration) of boron in carbonates should reflect the changing isotopic composition (and abundance) of aqueous borate ion with changing seawater pH. While this conceptual basis was initially supported by the similarity of the $\delta^{11}B$ of marine biogenic carbonates to that of borate ion (Hemming and Hanson, 1992), subsequent research has found that while the $\delta^{11}B$ of experimentally-precipitated synthetic aragonite does closely match that of aqueous borate ion (Noireaux et al., 2015), no synthetic calcites precipitated to date (Sanyal et al., 2000; Noireaux et al., 2015; Kaczmarek et al., 2016; Farmer et al., 2019) show as high a sensitivity of $\delta^{11}B$ to pH as would be predicted for aqueous borate ion using current estimates of the isotope fractionation between aqueous borate ion and boric acid (Klochko et al., 2006; Nir et al., 2015). Further, inorganically-precipitated calcite tends to mainly, but not exclusively (e.g see datapoint classified as an outlier by Noireaux et al., 2015) record $\delta^{11}B$ that is higher than the $\delta^{11}B$ of ambient borate ion ($\delta^{11}B_{borate}$). While deviations from the aqueous conceptual basis of the proxy in biogenic carbonates can often be attributed to physiological processes that decouple chemical conditions of $CaCO_3$ precipitation from bulk seawater chemistry, such as variable pH up-regulation in corals (e.g. Venn et al., 2013) or microenvironment alteration in foraminifera (e.g. Hönisch et al., 2003), inorganically-precipitated $CaCO_3$ is not subject to such vital effects, and as such the variability of results from synthetic carbonates challenges our current understanding. Furthermore, the reason why boron isotope incorporation behaviour should be so strongly dependent on polymorph is not fully understood.

One potential mechanism by which inorganic carbonates may be elevated relative to ambient borate ion is the incorporation of some amount of boric acid (which is isotopically heavier than borate ion). Since the isotopic fractionation between boric acid and borate ion is large (~26–27.2 ‰; Klochko et al., 2006; Nir et al., 2015), any potential contribution from boric acid in ancient calcites that was non-systematic would impede attempts to resolve past changes in ocean pH using the boron isotope composition of marine carbonate. Incorporation of both aqueous boron species has often been inferred based on nuclear magnetic resonance (NMR) studies showing boron in carbonates may be trigonally or tetrahedrally coordinated (e.g. Sen et al., 1994; Klochko et al., 2009; Mavromatis et al., 2015; Noireaux et al., 2015). Since aqueous boric acid is trigonally-coordinated, some have cited this trigonal coordination in carbonate as evidence of boric acid inclusion (e.g. Klochko et al., 2009; Cusack et al., 2015; Noireaux et al., 2015; Balan et al., 2016). However, the proportion of trigonal boron observed in carbonates correlates very poorly with measured elevation of $\delta^{11}B$ relative to borate ion (Branson et al., 2015; Noireaux et al., 2015), cautioning against directly equating NMR coordination to the original aqueous boron species that was incorporated (see also Sen et al., 1994).

An alternative line of argument for inclusion of both aqueous species in calcite comes from improved goodness-of-fit in observed synthetic calcites (but not aragonites; Holcomb et al., 2016) when boron partitioning is parameterised by λ_B ($\lambda_B = B/Ca_{carbonate}/([B]_{solution}/[\text{Dissolved Inorganic Carbon}]_{solution})$) rather than via aqueous borate concentration alone (e.g. Uchikawa et al., 2015). Indeed, Branson (2018), and subsequently Farmer et al. (2019), have had considerable success in explaining some (but not all) published boron isotope data from synthetic carbonates within a surface kinetic modelling (SKM) framework (building on DePaolo, 2011), involving both major aqueous boron species. In this model, the boron isotope composition of the precipitated mineral is determined by the balance between detachment and attachment rates of either species to the growing crystal face. Differences in boron isotope composition between experimental calcites and aragonites can thus be explained via a slower detachment rate of trigonal boric acid from the growing calcite face, and thus a greater propensity for retention of this isotopically-heavy species in the crystal lattice. This model can explain variability across the wide range of experimental treatments (pH, [DIC], [Ca^{2+}], and [B]) of Uchikawa et al. (2015; 2017), as well as much, if not all, published data from elsewhere (Mavromatis et al., 2015; Noireaux et al., 2015; Kaczmarek et al., 2016). While the SKM approach clearly appears to be very promising, there are outstanding questions that would benefit from the provision of more experimental data. For instance, it is not yet possible to conclusively distinguish whether published data are better explained via the Surface Entrapment Model (SEMO, where impurities in a surface boundary layer are trapped by rapid crystal overgrowth; Watson, 2004) or the SKM model. Also, intriguingly, structure in the residuals between SKM model predictions and experimental observations points to the existence of an as-yet-unidentified process that is not parameterised in the model, perhaps linked to a

secondary control on the availability of binding sites (Farmer et al., 2019). Additionally, adsorption experiments by Saldi et al. (2018) found little support for adsorption of trigonally coordinated boric acid to the calcite surface, which would make it difficult to envisage attachment rates of boric acid ever exceeding those of detachment, as the SKM would require. More fundamentally perhaps, the observed isotopic fractionations during adsorption of borate ion (Saldi et al., 2018) and modelled equilibrium fractionation between the solid carbonate and aqueous boron phases (Balan et al., 2016; Balan et al., 2018) call into question some of the fundamental assumptions of the SKM model and indeed of the boron isotope proxy in general.

To address these outstanding questions, we present new $\delta^{11}B$ data from experimentally-precipitated synthetic calcite and aragonite, measured via multicollector inductively-coupled plasma mass spectrometry (MC-ICPMS). These precipitates, grown without seed material at seawater-like ionic strength (I = 0.7 mol/kg) in the presence of Mg, expand the range of pH (~7.4–9.4) covered by previous published data. Careful monitoring of the oxygen isotope compositions of precipitates and parent water show they were formed at (or close to) oxygen isotope equilibrium with parent water (see Kim et al., 2014). Since B isotopic equilibrium is reached before O isotope equilibrium (Zeebe et al., 2001), a lack of non-equilibrium isotope effects for O isotopes should suggest a corresponding lack for B. Boron isotope measurements are coupled with measurements of other trace and minor element-Ca ratios, to place observed isotopic fractionations within a broader framework that also considers other interacting and/or competing ions. Finally, we also include the results of a reanalysis of the calcite precipitates of Sanyal et al. (2000) via MC-ICPMS, allowing greater ease of comparison with newer data, without necessitating consideration of possible analytical offsets in negative thermal ionisation mass spectrometry (NTIMS) data (e.g. Hönisch et al., 2003; Foster et al., 2013; Farmer et al., 2016).

2. METHODS

2.1. $CaCO_3$ precipitation via the Constant Addition Method

Methodology for calcite or aragonite precipitation largely followed Kim et al. (2014), with the addition of B ([B] = 7.9 mmol/kgw) in the growth medium. Starting experimental solutions for $CaCO_3$ precipitation experiments were prepared gravimetrically using deionized water (18.2 MΩ cm) and ACS grade $B(OH)_3$, NaCl and $NaHCO_3$ and/or Na_2CO_3, dependent on the intended starting pH of the experimental solution (all at $I = \sim 0.7$ mol/kgw). To ensure oxygen isotope equilibrium between the DIC species and water, solutions were left to equilibrate for a minimum of 7 days in a temperature-controlled water bath at 25 ± 0.01 °C. Immediately prior to beginning each synthesis experiment, ACS grade $MgCl_2{\cdot}6H_2O$ and $CaCl_2{\cdot}2H_2O$ were added to these isotopically-equilibrated starting solutions (see Table 1 for details). The ratio of [Mg] to [Ca] differed according to the desired polymorph in each experiment (Morse et al., 2007): aragonite was precipitated at a solution Mg:Ca of 4:1, but in order to precipitate calcite, solution Mg:Ca was lowered to 0.13:1. The addition of the hydrated chloride salts had no detectable influence on the oxygen isotopic composition of the growth medium, due to their relatively low concentrations. Starting solutions were then held in an airtight Teflon reaction chamber at 25.04 ± 0.03 °C (aragonite) or 25.00 ± 0.04 °C (calcite).

Precipitation of $CaCO_3$ began with the constant addition of two titrants (also of $I = 0.7$ mol/kgw), the first a NaCl and $NaHCO_3$ and/or Na_2CO_3 solution, the second a $CaCl_2{\cdot}2H_2O$, $B(OH)_3$, and NaCl solution (see Table 1). Both were prepared with deionized water from the same batch as that used in the starting solution to ensure consistency of $\delta^{18}O_{H2O}$. After nucleation, which is spontaneous and involves no seed material, precipitation rate and solution pH were paced by the steady rate of injection of two titrants (at 0.5 ml hr^{-1}). Because these experiments were carried out in sealed reaction vessels without a Ca electrode, exact timing of nucleation is not known. Based on prior experience during the development of the constant addition method (Kim et al., 2006; Kim et al., 2014), however, nucleation occurs soon after titration begins (at latest 24–48 hours). The composition of titrants was designed to keep pH stable during precipitation experiments, but where adjustments were necessary, 1 % HCl was added. Precipitation lasted between 67 and 627 hours from the onset of titration, depending on the experiment, yielding between 42 and 389 mg of $CaCO_3$ (Table 1). The pH of the growth medium was measured daily, using an NBS-calibrated potentiometric electrode. Within-run pH variability for experiments at medium-range pHs (~8.5–9) was often less than 0.1 pH units (at 2 sd), but was considerably larger for some low-pH experiments (up to 0.28 units, 2sd), as shown in Supp. Fig. 1. However, since this variability during the experiment is averaged out in the carbonate sample that is ultimately analysed, we take two standard error on the mean pH as our uncertainty. Note, for input to PHREEQC, these NBS pH values were converted to MacInnes convention pH (Nir et al., 2014).

Aliquots of the growth medium were taken for boron and oxygen isotope analysis at the beginning and end of each precipitation experiment, with samples for boron filtered through a 0.45 μm Millipore Durapore® syringe filter to remove any suspended crystalline material, and subsequently stored in acid-cleaned high-density polyethylene bottles. Upon collection of water samples, the remaining precipitation medium was run through a vacuum filtration system using 0.45 μm Durapore® membrane filters to isolate the suspended crystals. These were thoroughly rinsed with 2 L of 18.2 MΩ cm Milli-Q water to remove residue from the growth media, followed by ultra-pure methanol to remove water that might later interact with the carbonate, and oven-dried at ~ 70 °C overnight before weighing. Mineralogy of samples was screened using X-ray diffraction (XRD), with all experimental carbonates analysed here (with the possible exception of sample iMH15) found to consist of purely one polymorph (at least within the resolution of the technique). All measured XRD spectra are provided in Supplementary Appendix 2.

Table 1
Precipitation conditions and chemistry of growth media. Note, experiments were unseeded: the polymorph precipitated in each case was determined only by the ratio of Mg to Ca in the growth solutions. XRD analysis confirmed purity of polymorph in each case.

		Reactor volume	Duration	Mass precipitated	Precipitation rate	pH (NBS scale)			Starting Growth Medium Values						Titrant 1			Titrant 2			Amount of Titrants added
									$NaHCO_3$	Na_2CO_3	Ca	Mg	B	NaCl	$NaHCO_3$	Na_2CO_3	NaCl	Ca	B	NaCl	
Sample name	**Polymorph**	**L**	**hrs**	**mg**	**mg/hr**	**mean**	**2sd**	**2se**	**mMol/kgw**	**mMol/kgw**	**mMol/kgw**	**mMol/kgw**	**mMol/kgw**	**mMol/kgw**	**mMol/kgw**	**mMol/kgw**	**mMol/kgw**	**mMol/kgw**	**mMol/kgw**	**mMol/kgw**	L
CKG-Oct511	Aragonite	1	375.2	70.01	0.187	8.765	0.061	0.016	5	5	0.5	2	7.9	685	60	20	620	3	20	695	0.19
iMH1/1-Mar2112-C	Aragonite	1	411.1	45.33	0.110	8.780	0.049	0.014	5	5	0.5	2	7.9	685	60	20	620	3	20	695	0.21
iMH2/1-Apr2712-D	Aragonite	1	405.9	42.67	0.105	8.830	0.079	0.024	5	5	0.5	2	7.9	685	60	20	620	3	20	695	0.20
iMH3/1-Aug312-D2	Aragonite	2	406.9	263.51	0.648	9.326	0.099	0.018	0	10	0.25	1	7.9	685	0	80	510	5	20	695	0.20
iMH4/1-Aug3012-E	Aragonite	2	626.9	79.34	0.127	8.762	0.084	0.017	5	5	0.5	2	7.9	685	60	20	620	3	20	695	0.31
iMH5/1-Sept2512-D2	Aragonite	2	595.2	92.44	0.155	9.376	0.053	0.009	0	10	0.25	1	7.9	685	0	80	510	5	20	695	0.30
iMH6/1-Oct2912-E	Aragonite	2	595.2	71.39	0.120	8.717	0.046	0.010	5	5	0.5	2	7.9	685	60	20	620	3	20	695	0.30
iMH7/DEC512-D2	Aragonite	2	479.4	67.07	0.140	9.408	0.102	0.021	0	10	0.25	1	7.9	685	0	80	510	5	20	695	0.24
iMH8/FEB2513-C	Aragonite	2	450.8	75.21	0.167	9.425	0.110	0.022	0	10	0.25	1	7.9	685	0	80	510	5	20	695	0.23
iMH9/FEB2513-D	Aragonite	2	450.8	58.76	0.130	9.431	0.108	0.022	0	10	0.25	1	7.9	685	0	80	510	5	20	695	0.23
iMH10/FEB2513-E	Aragonite	2	283.0	389.06	1.375	7.452	0.246	0.066	10	0	10	40	7.9	570	60	20	620	10	20	695	0.14
iMH11/APR313-C	Aragonite	2	307.3	339.86	1.106	7.590	0.281	0.072	10	0	10	40	7.9	570	60	20	620	10	20	695	0.15
iMH12/APR313-D	Aragonite	2	211.6	334.98	1.583	7.562	0.228	0.066	10	0	10	40	7.9	570	60	20	620	10	20	695	0.11
iMH13/APR313-E	Aragonite	2	67.2	67.00	0.997	7.601	0.256	0.105	10	0	10	40	7.9	570	60	20	620	10	20	695	0.03
iMH14/OCT2912-E2	Aragonite	2	599.7	88.08	0.147	8.686	0.052	0.011	5	5	0.5	2	7.9	685	60	20	620	3	20	695	0.30
iMH15/DEC512-D	Aragonite	2	599.7	79.85	0.133	9.337	0.127	0.023	0	10	0.25	1	7.9	685	0	80	510	5	20	695	0.30
iMH16/DEC1/412-C	Aragonite	2	599.7	270.13	0.450	7.535	0.158	0.026	7.5	2.5	10	40	7.9	592	16	4	685	5	20	695	0.30
iMH17/0628C-MRS1	Calcite	2	358.5	100.00	0.279	8.400	0.244	0.063	7.5	2.5	1	0.13	7.9	692	16	4	685	10	20	685	0.18
iMH18/0628D-MRS1	Calcite	2	358.5	92.00	0.257	8.580	0.149	0.039	7.5	2.5	1	0.13	7.9	692	16	4	685	10	20	685	0.18
iMH19/0628E-MRS1	Calcite	2	358.5	110.00	0.307	8.700	0.247	0.064	7.5	2.5	1	0.13	7.9	692	16	4	685	10	20	685	0.18
iMH20/0730D-MRS1	Calcite	2	594.8	91.00	0.153	8.460	0.068	0.015	7.5	2.5	1	0.13	7.9	692	16	4	685	10	20	685	0.30
iMH21/0730E-MRS1	Calcite	2	594.8	113.00	0.190	8.420	0.151	0.032	7.5	2.5	1	0.13	7.9	692	16	4	685	10	20	685	0.30
iMH23/1112A-MRSI	Calcite	2	452.2	330.00	0.730	7.400	0.242	0.061	10.0	0.0	10	1.30	7.9	673	20	0	690	10	20	685	0.23
iMH24/1112C-MRSI	Calcite	2	452.2	325.00	0.719	7.430	0.231	0.058	10.0	0.0	10	1.30	7.9	673	20	0	690	10	20	685	0.23
iMH25/1204A-MRSI	Calcite	2	385.3	212.00	0.550	7.460	0.208	0.054	10.0	0.0	10	1.30	7.9	673	20	0	690	10	20	685	0.19
iMH26/1204C-MRSI	Calcite	2	385.3	188.00	0.488	7.460	0.195	0.050	10.0	0.0	10	1.30	7.9	673	20	0	690	10	20	685	0.19

2.2. Oxygen isotope analysis

Oxygen isotope compositions of calcium carbonate samples were determined using a VG OPTIMA isotope ratio mass spectrometer at McMaster University, equipped with an ISOCARB automated common acid bath at 90 °C, with a 1σ uncertainty on $\delta^{18}O$ measurements of ± 0.08 ‰. The measured $\delta^{18}O$ values of acid-liberated CO_2 ($\delta^{18}O_{CO2(ACID)}$) from two reference materials (NBS 18 and NBS 19) at 90 °C were fitted against the $\delta^{18}O_{CO2(ACID)}$ value of 17.48 ‰ (NBS 18) and 39.19 ‰ (NBS 19). The measured $\delta^{18}O_{CO2(ACID)}$ value from each sample was then normalized using the relationship obtained above, and the acid fractionation factor of 1.01063 for aragonite or 1.01030 for calcite at 25 °C (Kim et al., 2007) was used to calculate the oxygen isotope composition of synthetic aragonite ($\delta^{18}O_{Aragonite}$) or calcite ($\delta^{18}O_{Calcite}$).

For oxygen isotope analysis of water samples, a modified CO_2-H_2O equilibration technique (Epstein and Mayeda, 1953) was employed using a Gas Bench II headspace autosampler and a Thermo Finnigan DeltaPlus XP Isotope Ratio Mass Spectrometer (IRMS) at McMaster University. Exetainer® glass vials were flushed and filled with a 0.2 % CO_2 and 99.8 % He mixture with a double needle at a flow of 100 ml min^{-1}. 0.2 ml of water sample was injected into each glass vial, allowing ≥ 27 hr to equilibrate at 25 ± 0.1 °C before the CO_2 in the headspace was analyzed by IRMS. Samples were analyzed in duplicate with in-house water standards MRSI-STD-W1 and MRSI-STD-W2 ($\delta^{18}O$ = −0.58 ‰ and −28.08 ‰ respectively). Uncertainty on water $\delta^{18}O$ measurements is ± 0.05 ‰ (1σ).

2.3. Boron isotope analysis

All boron isotope analyses were carried out at the University of Southampton (UoS), using multi-collector inductively-coupled plasma mass spectrometry (MC-ICPMS), following Foster (2008) and Henehan et al. (2013). As is critical for inorganic precipitation experiments such as these, sample precipitates were cleaned thoroughly to ensure complete removal of any boron that may have adhered to the mineral surface from the experimental medium. Specifically, having been rinsed with 2 L of MilliQ water before drying and transportation, carbonate samples were then rinsed five times with ∼ 500 µL of boron- free MilliQ water, ultrasonicated (30 s) and centrifuged (4 mins). Each time, supernatant was extracted, acidified, and analysed for B/Ca on a Thermo X-Series II Quadropole ICPMS to verify the efficiency of rinsing, and to ensure the analysed carbonate was free of adsorbed B (see Supp. Fig. 2). Carbonate samples were then transferred to Teflon centrifuge tubes, subjected to a weak acid leach (0.0005 M HNO_3) to remove any adsorbed contaminants, rinsed three times more to remove the weak acid, and finally dissolved via stepwise addition of 0.5 M HNO_3. For each sample, a 20 µl aliquot of dissolved material was taken for trace and minor element/Ca ratio analysis (see Section 2.4). Samples of the experimental medium were acidified with HNO_3 and ultrasonicated prior to analysis to ensure any possible precipitates were redissolved. Subsequently, separation of B from matrix prior to analysis via ion chromatography followed Henehan et al. (2013).

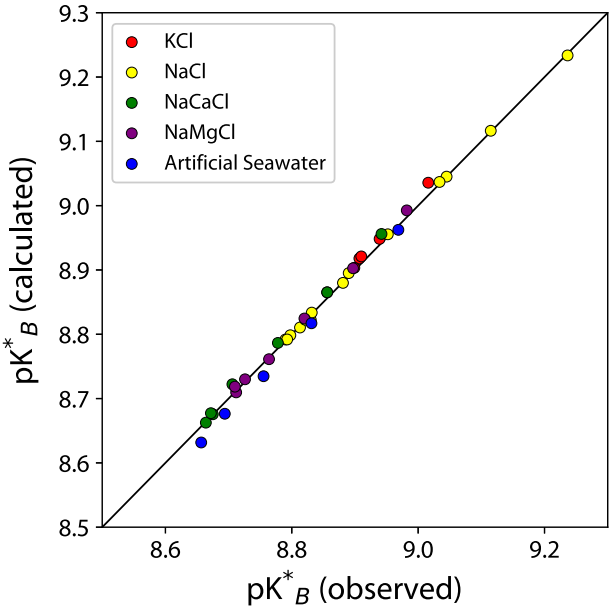

Fig. 1. Values of pK^*_B calculated by the Pitzer database within PHREEQC (Parkhurst and Appelo, 2013) agree well with empirical observations across a broad range of ionic strengths (0–6.15 M) in KCl solutions (Dickson, 1990b), NaCl solutions (Owen and King, 1943; Hershey et al., 1986), Na-Mg-Cl and Na-Ca-Cl solutions (Hershey et al., 1986), and even artificial seawater, once corrected from total scale (Dickson, 1990a). Since our solution chemistries (Na-Mg-Ca-B-Cl) are intermediate between those of Hershey et al. (1986) and Dickson (1990a), the Pitzer database can be considered appropriate for use here, as well as in recalculation of published data.

Analytical uncertainty was estimated with reference to repeat analyses of JCp-1 coral aragonite standard (Okai et al., 2002) measured at UoS on 10^{11} Ω amplifiers, using the relationship between 2σ external reproducibility and ^{11}B signal intensity from Henehan et al. (2013). Typical long-term reproducibility was < 0.23 ‰ (2sd) for 20 ng B and < 0.33 ‰ (2sd) for 4 ng B.

2.4. Trace and Minor Element/Ca ratios

Trace and minor element/Ca ratios were measured on an aliquot of the same dissolved sample material as was analysed for boron isotope ratios, using a Thermo Element ICP-MS at UoS. Measurement methods are detailed in Henehan et al. (2015). Reproducibility of element/Ca ratio measurements was gauged by repeat measurement of three in-house consistency standards (B/Ca ratios of 197, 496, and 32 µmol/mol, respectively) with these sample runs, and was 6 % for B/Ca, 1 % for Na/Ca and 2 % for Mg/Ca (all at 2 sd).

2.5. Aqueous boron and carbonate speciation calculations

Since the parameterization of pK^*_B (the equilibrium constant between boric acid and borate ion in solution)

typically used in boron isotope-pH reconstructions (Dickson, 1990a) is based on 'normal' seawater chemistry, it is not applicable to the Na-Ca-Mg-Cl solutions used here. Approaches taken to address this issue in previous studies have varied and may contribute to the variability observed between studies. Kaczmarek et al. (2016) and Noireaux et al. (2015) used the MINTEQA2 database, within the framework of PHREEQC (Parkhurst and Appelo, 2013) to calculate aqueous speciation. While this database uses the Davies equations (Davies, 1938) to extend Debye–Hückel parameters to higher ionic strengths than their original derivations, these equations are still not intended for use at ionic strengths greater than ~ 0.5 M. Consequently, while for the low ionic strength growth media (0.1–0.2 M) of Noireaux et al. this should not introduce significant error, for the higher ionic strength experiments of Kaczmarek et al. this database is not suitable. The MyAMI model (Hain et al., 2015), itself developed from the MIAMI Ionic Interaction Model (Millero and Pierrot, 1998), can be used to calculate pK^*_B and carbonate equilibrium constants for palaeo-seawater with different [Ca] and [Mg], but at unusual ionic strengths and solution chemistries far removed from seawater it produces values of pK^*_B that diverge significantly from experimentally determined values (Farmer et al., 2019). Instead, Farmer et al. (2019) used the Pitzer database (pitzer.dat) implemented within PHREEQC (Parkhurst and Appelo, 2013) because the output pK^*_B values best fit measured observations across a range of experimental solution chemistries, notwithstanding some divergences between calculated and observed pK^*_B values in artificial seawater. Following these authors, we also use the Pitzer database here, but we note that when one accounts for the fact that empirical artificial seawater pK^*_B values (Dickson, 1990a) are reported on the total scale, and calculation of pK^*_B from speciation in PHREEQC is based on the free scale (or more specifically, MacInnes convention pH; Nir et al., 2014), the fit between Pitzer-calculated pK^*_B and empirical pK^*_B (Fig. 1) is in fact even better than was reported by Farmer et al. (2019).

Our speciation calculations use concentrations of ions in precipitation media, as determined both from gravimetric measurements of starting reagents and titrants, and from gravimetric (mass of dried $CaCO_3$) and geochemical (from measured Na/Ca, B/Ca and Mg/Ca ratios in $CaCO_3$) quantification of ions removed in precipitates over the course of the experiments. These concentrations are given in Supplementary Table 1. Although the concentrations of some ions (e.g. Na, B) varied somewhat through each of our precipitation experiments, the resultant change in $\delta^{11}B_{borate}$ due to these variations was less than 0.1 ‰. Nonetheless for our study and for the study of Kaczmarek et al. (2016) we incorporate uncertainty in calculated pK^*_B and Saturation Index (SI; $SI = \log_{10}((\text{Ionic Activity Product})/(\text{Polymorph solubility constant } K_{sp}))$ due to changing major ion concentrations, along with variability in growth medium pH and uncertainty in growth medium $\delta^{11}B$, via a Monte Carlo approach. Specifically, 2,000 simulated datasets were generated within a uniform distribution between starting major ion concentrations and their corresponding concentrations at the end of each experiment (accounting for solute loss into the precipitates), and from normal distributions within pH and $\delta^{11}B_{solution}$ uncertainty. Speciation was then calculated for each Monte Carlo solution using the PhreeqPy implementation of PHREEQC in Python (https://phreeqpy.com), which is in turn facilitated by IPhreeqc (Charlton and Parkhurst, 2011a), and boron isotope calculations calculated with reference to absolute isotope ratios (Rae, 2018) using modified formulations of code used by Farmer et al. (2019) and made available by O. Branson (https://github.com/oscarbranson).

2.6. Quantifying precipitation rate

Published experimental data (Uchikawa et al., 2015; Kaczmarek et al., 2016; Uchikawa et al., 2017) have highlighted the importance of precipitation rate (R) in controlling boron incorporation. While we have no Brunauer–Emmett–Teller (BET)-based estimate of surface-area normalised precipitation rate for our experiments, we can calculate a number of other (albeit imperfect) indicators of precipitation rate that can be compared to geochemical results. Amongst these, estimates of bulk precipitation rate (i.e., mass of carbonate precipitated per hour) should be most indicative of the crystal-scale growth rate, even if other factors relating to crystal form likely make this an imperfect proxy. Indeed, in studies where area-normalised precipitation rate is available, this correlates reasonably well with the bulk precipitation rate metric we use here (Supp. Fig. 3). Other possible indicators of crystal-scale growth rate include SI, which should strongly influence precipitation rate (Zhang and Nancollas, 1998). However, since in our experiments growth medium Mg concentrations varied, potentially variable retardation effects on (particularly calcite) crystal growth (e.g. Berner, 1975; Nielsen et al., 2016) between experiments mean using SI as a proxy for precipitation rate may also not be straightforward. Indeed, we note that for our experiments, precipitation rate in mg hr^{-1} is negatively correlated with pH and SI (Supp. Fig. 4). For this same reason, it is not possible to use the relationship between observed R and SI from Uchikawa et al. (2015; 2017) to estimate surface area-normalised growth rate following Farmer et al. (2019), as their experimental solutions did not contain Mg. Furthermore, their relationship based on calcite precipitation experiments is likely not applicable to our aragonites. Alternatively, others have noted the influence of $[Ca^{2+}]/[CO_3^{2-}]$ as a primary control on calcite growth rate when saturation is otherwise held roughly constant (Nehrke et al., 2007; van der Weijden and van der Weijden, 2014), and ability of the $CaCO_3$ product/sum ratio to predict growth rate of Mg-rich amorphous $CaCO_3$ (ACC) when Ω varies (Evans et al., 2020), and so we consider these here as other possible indicators of crystal growth rates in our experiments (noting that both correlate well with bulk precipitation rate, our preferred metric; Supp. Fig. 5).

2.7. Reanalysis of Sanyal et al. (2000) carbonates

For information regarding the precipitation experiments of Sanyal et al. (2000), we refer the reader to the original

publication. Although not stated by Sanyal et al. (2000), the artificial seawater used in their study followed the recipe of Kester et al. (1967), but with the omission of Mg, and some alteration of [Ca] to moderate precipitation rates (J. Bijma, pers. comm.). Records of the exact values of [Ca] are no longer available, and thus in the absence of better estimates we assume seawater [Ca] in speciation calculations here, with the proviso that these values are likely inaccurate. MC-ICPMS and ICPMS analyses were carried out at the University of Bristol, following the methods of Foster (2008), and with uncertainty on these data being two standard deviations of four replicate measurements. B/Ca ratios in the first three rinse steps were measured to assess efficacy of cleaning, before a subsequent weak acid leach and three further Milli-Q leaches. While after three rinses B/Ca ratios in the rinse solutions levelled off somewhat, we cannot be certain that these rinses were sufficient (see Supplementary Appendix A for full discussion). Hence, given this uncertainty, and that surrounding [Ca] in the growth media, we refrain from over-interpreting these data in this study.

3. RESULTS

3.1. Experimental conditions and equilibrium fractionation

Details of conditions during each precipitation experiment, along with masses of resultant precipitate and precipitation rates, are given in Table 1. For further details of the evolution of growth medium chemistry, see the Supplementary Table 1. Precipitation rates based on total mass precipitated range from 0.11 to 1.58 mg/hr for aragonites, and 0.15 to 0.73 mg/hr for calcites. The observed oxygen isotope fractionation of synthetic aragonites ($1000\ln\alpha_{aragonite\text{-}water}$) ranges between 28.80 and 29.15 ‰ (Table 2), within analytical uncertainty of the published estimate of 28.87 ± 0.13 ‰ at the same ionic strength of I = ~0.7 mol/kg reported by Kim et al. (2014). Calcite samples are however systematically offset by ~ 0.5–0.7 ‰ (i.e. beyond combined 2σ analytical uncertainty of 0.19 ‰) from the equilibrium calcite-water fractionation proposed by Kim and O'Neil (1997) using not only a different technique of carbonate precipitation – where supersaturation of the precipitation medium was reached by bubbling N_2 gas to forcibly degas CO_2 – but also a much lower ionic strength. This offset is not strongly correlated with pH or SI, or [Ca]/[DIC] in either aragonite or calcite precipitation experiments (see Supp. Fig. 6).

3.2. Trace element ratios

Minor (Na, Mg, Sr) and trace (B, Mn, Cd, Ba, U, Nd, Al) element-Ca ratios are listed in Table 2 and Supplementary Table 2. Note however that of these elements, only Na, Mg, and B were intentionally and quantifiably added to the growth media; other elements could only have been introduced as impurities in original reagents, or via contamination from experimental apparatus. We provide these data in the supplement for posterity, but since it is inadvisable to over-interpret the distribution of elements whose concentrations in the experimental fluid were not controlled, we do not discuss these further. Observed Na/Ca ratios in aragonites ranged from 9 to 32 mmol/mol, compared to only 2–8 mmol/mol in calcites, confirming a higher affinity for Na in aragonite observed elsewhere (Kitano et al., 1975). B/Ca ratios are also similarly higher in aragonite (350–1852 μmol/mol) than calcite (107–315 μmol/mol), in agreement with previous studies (e.g. Furst et al., 1976; Kitano et al., 1978; Noireaux et al., 2015). Conversely, despite higher aqueous [Mg] in aragonite growth media, Mg/Ca ratios were often higher in calcites (2.6–5.1 mmol/mol) than aragonites (0.9–6.0 mmol/mol), as observed elsewhere (e.g. Berner, 1975).

B/Ca ratios (Fig. 2a) and elemental partitioning (expressed here as λ_B, defined above, Fig. 2b) are significantly positively linearly correlated with experimental pH for both aragonite ($R^2_{B/Ca}$ = 0.29, $R^2_{\lambda B}$ = 0.39) and calcite ($R^2_{B/Ca}$ = 0.74, $R^2_{\lambda B}$ = 0.73). Na/Ca ratios are similarly positively correlated with pH (Fig. 2d) in both aragonite ($R^2_{Na/Ca}$ = 0.67) and calcite ($R^2_{Na/Ca}$ = 0.93). However, when one accounts for the considerable range in growth medium Na/Ca, partitioning of Na (i.e. $D_{Element}$: $Element/Ca_{solid}/Element/Ca_{solution}$) into the solid form is in fact lower when pH is higher (Fig. 2e). Mg/Ca (Fig. 2g) shows little response to pH in calcites, but when changing solution [Mg] between experiments is accounted for (D_{Mg}; Fig. 2h, i), there is an evident increase in Mg partitioning into aragonite at higher pH/SI. Because in our experiments calculated SI was linearly correlated with pH (R^2_{calc} = 0.60, p_{calc} = 0.01; R^2_{arag} = 0.50, p_{arag} < 0.01; Supp. Fig. 7), similar trends for each element are seen against SI (Fig. 2 c, f, i), although in most cases the correlations are weaker than for pH.

While these relationships highlight the predominant control of the carbonate system on boron incorporation, there is clearly considerable residual variability around these relationships, with individual aragonite precipitate B/Ca values varying by ~ 1000 μmol/mol even within very similar low pH treatments. Note that the strength of the carbonate system control on B/Ca is not any more significant when plotted against calculated $[B(OH)_4^-]/[HCO_3^-]$, $[B(OH)_4^-]/[DIC]$ or $[B(OH)_4^-]/[CO_3^{2-}]^{0.5}$, and so we plot against pH as the least derived (and hence least uncertain) parameter here (see Supp. Fig. 10 for alternative parameterisations). Similarly, we cannot discern whether there is any better fit between λ_B (plotted here following Uchikawa et al. (2015)) or $[B(OH)_4^-]/[DIC]$, although it is perhaps notable that our calcites and those remeasured values of Sanyal et al. (2000) fall on a similar trend when $[B(OH)_4^-]/[DIC]$ is used (Supp. Fig. 10). Given published experimental data point to precipitation rate (R) being important in controlling boron incorporation (Uchikawa et al., 2015; Kaczmarek et al., 2016; Uchikawa et al., 2017), one might predict residual variation from a relationship with the carbonate system in our experiments to be correlated with precipitation rate. Despite this, although our metrics for precipitation rate (bulk precipitation rate, SI, or $[Ca]/[CO_3^{2-}]$) may be imperfect substitutes for BET-based surface-area normalised precipitation rate (as we discuss in Section 2.6), it is striking that there is no correlation between *any* of these growth-rate metrics and residual

Table 2
Measured carbonate oxygen isotope fractionation, El/Ca ratios and $\delta^{11}B$, and measured growth medium $\delta^{11}B$. Note, since we see no evidence of any isotopic fractionation outside of uncertainty during experiments, or variability between experiments, we did not measure every growth medium solution before and after precipitation. Rather, we take the mean and 2se of all growth medium $\delta^{11}B$ measurements as the parent solution value (and associated uncertainty) for all carbonates. Uncertainty on B/Ca measurements is 6%, and for Mg/Ca and Na/Ca is 2%, based on repeat measurements of in-house standards during the relevant analytical runs.

		pH (NBS scale)		Carbonate Oxygen Isotope Fractionation 1000lnα		Carbonate			Carbonate		Starting Solution		End Solution		Carbonate normalised to sw = 39.61 ‰
Sample name	Polymorph	mean	2se	(‰)	± 1σ	B/Ca μmol/mol	Na/Ca mmol/mol	Mg/Ca mmol/mol	$\delta^{11}B$ (‰)	Ext. rep. (‰, 2sd)	$\delta^{11}B$ (‰)	Ext. rep. (‰, 2sd)	$\delta^{11}B$ (‰)	Ext. rep. (‰, 2sd)	$\delta^{11}B$ (‰)
CKG-Oct511	Aragonite	8.765	0.016	28.99	0.09	1061	19.875	1.197	−28.36	0.18			−14.39	0.18	24.83
iMH1/1-Mar2112-C	Aragonite	8.780	0.014	28.92	0.09	1174	21.515	1.240	−28.58	0.19	−14.31	0.22	−14.40	0.22	24.60
iMH2/1-Apr2712-D	Aragonite	8.830	0.024	28.92	0.09	1187	22.114	1.319	−28.70	0.19	−14.21	0.22	−14.35	0.22	24.47
iMH3/1-Aug312-D2	Aragonite	9.326	0.018	29.09	0.09	1858	21.885	6.035	−22.28	0.17	−14.45	0.22	−14.48	0.22	31.24
iMH4/1-Aug3012-E	Aragonite	8.762	0.017	28.90	0.09	750	16.018	1.034	−28.74	0.20	−14.33	0.22	−14.49	0.22	24.43
iMH5/1-Sept2512-D2	Aragonite	9.376	0.009	28.88	0.09	1077	20.985	2.388	−19.50	0.17	−14.30	0.22	−14.33	0.22	34.17
iMH6/1-Oct2912-E	Aragonite	8.717	0.010	28.84	0.09	1314	23.111	1.307	−28.54	0.18	−14.35	0.22	−14.35	0.20	24.63
iMH7/DEC512-D2	Aragonite	9.408	0.021	28.89	0.09	969	18.130	2.525	−18.99	0.18					34.71
iMH8/FEB2513-C	Aragonite	9.425	0.022	29.02	0.09	1048	19.517	1.994	−18.85	0.19	−14.25	0.16			34.86
iMH9/FEB2513-D	Aragonite	9.431	0.022	28.97	0.09	1477	27.365	3.656	−18.96	0.19					34.74
iMH10/FEB2513-E	Aragonite	7.452	0.066	29.08	0.09	349	7.953	1.008	−38.53	0.26					14.10
iMH11/APR313-C	Aragonite	7.590	0.072	29.10	0.09	912	13.968	1.412	−37.90	0.19	−14.35	0.19			14.77
iMH12/APR313-D	Aragonite	7.562	0.066	29.05	0.09	695	11.308	0.976	−38.06	0.19			−14.33	0.19	14.59
iMH13/APR313-E	Aragonite	7.601	0.105	29.01	0.09	1406	16.817	2.029	−37.99	0.19					14.67
iMH14/OCT2912-E2	Aragonite	8.686	0.011	28.80	0.09	862	17.128	1.654	−28.68	0.20					24.48
iMH15/DEC512-D	Aragonite	9.337	0.023	28.84	0.09	1110	22.446	3.614	−19.00	0.19	−14.51	0.20			34.70
iMH16//DEC1412-C	Aragonite	7.535	0.026	29.15	0.09	617	8.139	1.091	−37.28	0.21					15.42
iMH17/0628C-MRS1	Calcite	8.400	0.063	28.44	0.09	168	3.714	4.345	−31.01	0.25	−14.31	0.20			22.03
iMH18/0628D-MRS1	Calcite	8.580	0.039	28.53	0.09	298	3.695	2.979	−31.70	0.22			−14.28	0.19	21.30
iMH19/0628E-MRS1	Calcite	8.700	0.064	28.49	0.09	246	3.476	4.728	−30.13	0.21			−14.24	0.19	22.96
iMH20/0730D-MRS1	Calcite	8.460	0.015	28.42	0.09	267	3.465	2.428	−31.10	0.21	−14.27	0.20			21.94
iMH21/0730E-MRS1	Calcite	8.420	0.032	28.59	0.09	171	2.778	4.521	−29.71	0.22			−14.27	0.20	23.39
iMH23/1112A-MRSI	Calcite	7.400	0.061	28.66	0.09	117	1.391	4.728	−34.60	0.23			−14.29	0.19	18.25
iMH24/1112C-MRSI	Calcite	7.430	0.058	28.73	0.09	126	1.365	4.697	−34.78	0.21	−14.29	0.19			18.06
iMH25/1204A-MRSI	Calcite	7.460	0.054	28.59	0.09	109	1.385	4.617	−34.49	0.22	−14.27	0.20			18.36
iMH26/1204C-MRSI	Calcite	7.460	0.050	28.66	0.09	112	1.294	4.545	−34.83	0.26			−14.27	0.16	18.00

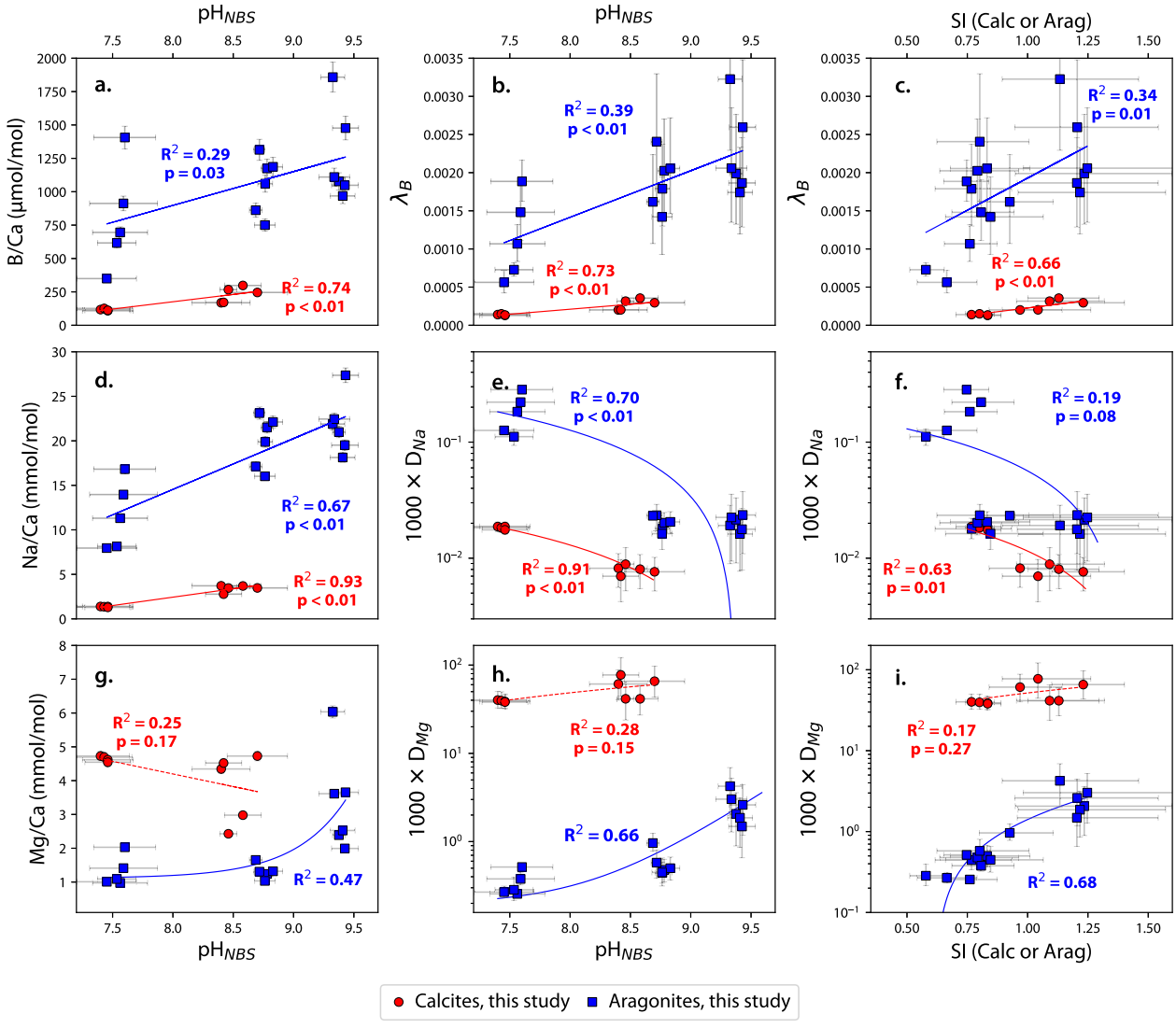

Fig. 2. The observed response of B, Na and Mg incorporation to changes in the carbonate system. Both B/Ca (panel a) and Na/Ca (panel d) ratios increase with pH in both aragonites (blue squares) and calcites (red circles). Because B/DIC did not vary significantly in the experiments, this is equally evident in λ_B values ($\lambda_B = B/Ca_{carbonate}/([B]_{solution}/[DIC]_{solution})$), shown in panel e. By contrast, because Na/Ca ratios in the growth medium vary considerably, pH appears to promote Na incorporation when plotted as raw Na/Ca ratios (panel d), but in fact partitioning of Na into the solid form (D_{Na}) is lower when pH is higher (panel e). Regression fits shown are based on the median slope and intercept of 2000 Monte Carlo datasets sampled within normal distributions of uncertainty around x and y variables, and stated statistics are the median R^2 and p-values of these Monte Carlo fits. The aragonite fits in panels g-i are exceptions to this: these are least-squares exponential fits through the central tendencies of the data, as linear fits resulted in considerably worse goodness-of-fit. For these fits, meaningful p-values could not be calculated. The form of regression fit applied was chosen to maximise R^2. See Supp. Fig. 8 for panel h plotted on a linear scale, and Supp Fig. 9 for a version of this Figure also including remeasured values of calcites from Sanyal et al. (2000). (For interpretation of the references to colour in this figure legend, the reader is referred to the web version of this article.)

variability from our observed B/Ca-pH relationship (Fig. 3-a-d). Neither is there any correlation with the ratio of growth-inhibiting Mg to carbonate ion (Fig. 3e), the boron concentration of the solution (which might induce disproportional increase in B incorporation; Allen and Hönisch, 2012) (Fig. 3f), the ionic strength of the solution (which might enhance B incorporation; e.g. Kitano et al., 1978) (Fig. 3g), or ($[Ca^{2+}]$*$[CO_3^{2-}]$)/($[Ca^{2+}]$ + $[CO_3^{2-}]$), found to be a useful predictor of ACC precipitation rate by Evans et al. (2020) (Fig. 3h). Finally, there is no correlation between residual B/Ca variability and the degree to which these carbonate samples diverged from oxygen isotope equilibrium (Supp. Fig. 11), which again suggests kinetics are not the dominant factor dictating B incorporation in our experiments.

Despite there being little correlation between residual B/Ca and experimental parameters, there is a strong correlation, consistent across both polymorphs ($R^2_{Calc} = 0.74$; $R^2_{Arag} = 0.64$), between B/Ca and Na/Ca (Fig. 4a), which in the case of aragonite is much stronger than the relation-

ship between either element and any carbonate system or saturation parameter. This apparent importance of Na/Ca is also evident in strong correlations between residual B/Ca variability around the pH trend and Na/Ca, particularly in aragonite (Fig. 4b). When such a consistent B/Ca-Na/Ca relationship is observed across both polymorphs, without an evident causal driver among solution chemistry parameters, one might infer some artefact of analysis or sample preparation. However, our sample cleaning protocol was consistent across all samples, and variability does not correspond to different analytical or sample preparation batches. Furthermore, there is little support for inaccuracy of matrix matching between sample and standard during ICPMS analysis (which may bias measurements of B/Ca; Yu et al., 2005) introducing significant residual variability in B/Ca (Supp. Fig. 12).

3.3. Boron isotopes

Boron isotope compositions of experimental solutions and precipitates are given in Table 2. We observed no difference outside of analytical uncertainty in solution $\delta^{11}B$ between experiments, and no systematic drift in $\delta^{11}B$ within individual experiments (Table 2). Therefore, for calculating aqueous $\delta^{11}B_{borate}$ and interpreting our data we assume a value of -14.34 ± 0.03 ‰ (2se), which is the mean and two standard errors of our solution measurements ($n = 31$). Measured carbonate $\delta^{11}B$ values range from -18.85 to -38.53 ‰. To aid comparison of our experimental data with other experimental data and data from natural carbonates, we normalise all carbonate data to a natural seawater $\delta^{11}B$ of 39.61 ± 0.04 ‰ (Foster et al., 2010), using the approach for dealing with modified seawater outlined by Zeebe and Wolf-Gladrow (2001). Since [Mg] and [Ca] (and hence pK^*_B) varied between our experiments, and between published experiments, $\delta^{11}B_{CaCO3}$ is plotted as a function of $\delta^{11}B_{borate}$ in Fig. 5 rather than pH, alongside our new measurements of Sanyal et al. (2000)'s precipitates, existing published data from Noireaux et al. (2015), Kaczmarek et al. (2016) and Farmer et al. (2019). Our new measurements of Sanyal et al. (2000)'s carbonates are broadly similar to the original NTIMS data at high pH, but diverge at low pH, giving a pH sensitivity (i.e. a slope) that is much closer to aqueous borate than previous data suggested (0.99 vs. 0.83; Fig. 5 and Supplementary Appendix), with the aforementioned caveat that we cannot confirm the efficacy of our rinses. For our own carbonates, as documented by Noireaux et al. (2015) over a more limited range in solution pH, we observe that $\delta^{11}B_{aragonite}$ closely follows that of $\delta^{11}B_{borate}$, but that $\delta^{11}B_{calcite}$ diverges progressively from $\delta^{11}B_{borate}$ as pH decreases, with a slope (i.e. a pH sensitivity) of considerably less than unity ($m=\sim0.5$). That said, our calcite data sit closer to the $\delta^{11}B_{borate}$ line than other previous inorganic calcite precipitates (Fig. 5). Also similar to Noireaux et al. (2015), we observe a slope that is slightly less than 1 for the fit between $\delta^{11}B_{aragonite}$ vs. $\delta^{11}B_{borate}$ calculated from an equilibrium fractionation factor between boric acid and borate (α_B, sometimes denoted $^{11\text{-}10}K_B$) of 1.0272 (Klochko et al., 2006; see Fig. 5a), and a slightly better fit with the 1:1 line for an α_B of 1.026 (Nir et al., 2015; see Fig. 5b). Indeed, to quantitatively determine the best fit of α_B to the combined body of aragonite data from Noireaux et al. (2015) and our aragonite data (accounting for uncertainty in each datapoint), we used SciPy.optimization (SciPy 1.0 Contributors et al., 2020), and derive an α_B of 1.02607: strikingly similar to that proposed independently by Nir et al. (2015).

4. DISCUSSION

4.1. Elemental partitioning: Na and Mg

The reduction in Na partitioning into both calcite and aragonite we observe with increasing pH (Fig. 2) is counter to the observations of Busenberg and Plummer (1985), who precipitated synthetic calcites from Na-Ca-S-K-Cl solutions with the stated aim of investigating the link between growth rate and Na incorporation. Their study revealed a similarly positive correlation between Na incorporation and pH, but in their study Na partitioning (D_{Na}) also increased with pH or SI. We also see a positive trend in D_{Na} with pH, albeit to a lesser extent, in the remeasured calcites of Sanyal et al. (2000) (Supp. Fig. 13). Busenberg and Plummer (1985) concluded that the incorporation of Na a) followed a Freundlich isotherm (indicative of adsorption behaviour, rather than straightforward Nernst partitioning), b) increased with growth rate ($R^2 = 0.25$, $p = 0.04$), c) was linked to the number of defect sites in the calcite structure, and d) itself increases the lattice spacing of the calcite. These latter two observations are supported by subsequent research which reproduced a rate effect on Na partitioning (Mucci, 1988) and demonstrated that Na is hosted in substitutional defect sites, not interstitial sites (Yoshimura et al., 2017). The decrease in D_{Na} we observe with pH and SI could therefore simply be a result of lower bulk precipitation rates (in mg/hr) in our higher pH/SI calcite and aragonite experiments (Supp. Fig. 4), in contrast to a strongly positive correlation ($R^2 = 0.79$, $p < 0.01$) between pH and precipitation rate in Busenberg and Plummer's experiments. However, if this implies that our bulk precipitation rate estimates are indeed an accurate proxy for crystal-surface-scale precipitation rate, this has implications for our boron incorporation/isotope data (discussed later). Additionally, we note that Füger et al. (2019) observed a similar negative trend in Na partitioning with pH, which they attributed not to changing precipitation rate, but a lower prevalence of HCO_3^- ion to be incorporated into the $CaCO_3$ lattice to balance the incorporation of monovalent Na^+. This effect would not be apparent in the experiments of Busenberg and Plummer (1985), because their experimental pH never reached values high enough for carbonate speciation to begin to move from HCO_3^- to CO_3^{2-}. It is unlikely, then, that Na partitioning is a straightforward reflection of precipitation rate alone.

In the case of Mg, we see little change in partitioning in calcite with pH or SI, but we observe higher D_{Mg} with higher pH/more saturated conditions in aragonites (Fig. 2h,j). However, in light of inconsistent responses of Mg partitioning to precipitation rate in published aragonite

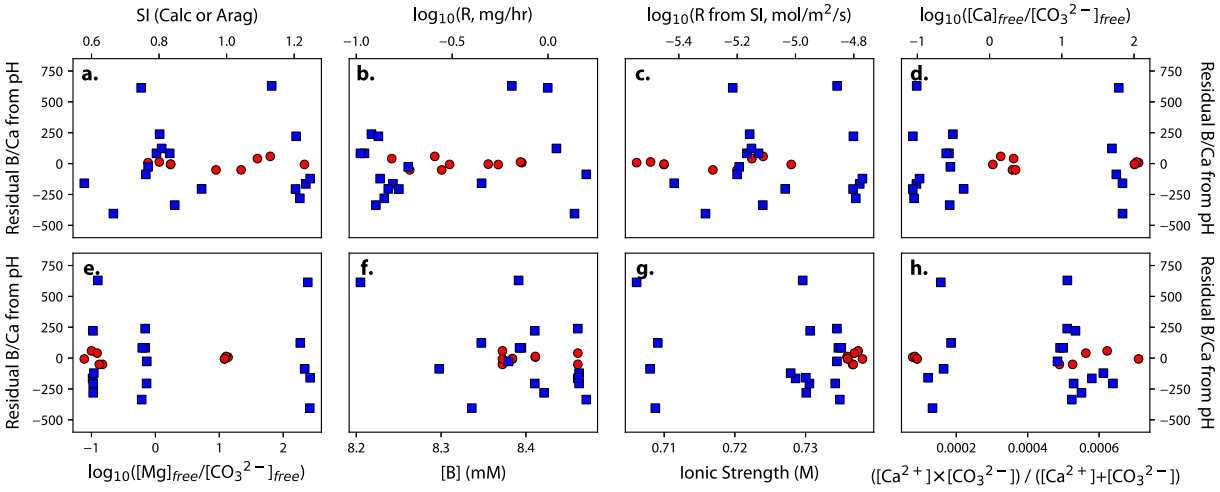

Fig. 3. Residual variability from the B/Ca-pH relationship observed in Fig. 2a against experimental solution and measurement parameters. As in Fig. 2, calcites are shown as red circles, and aragonites as blue squares. No correlations are observed between (a) solution Saturation Index (note aragonites plotted against SI_{arag}, calcites vs. SI_{calc}), (b) precipitation rate parameterized as mass of carbonate grown per hour, (c) precipitation rate based on the relationship between SI and R following Farmer et al. (2019), (d) Calcium to carbonate ion ratio, (e) Mg concentrations relative to carbonate ion, (f) total boron concentration in solution, (g) ionic strength or (h) $CaCO_3$ product over sum.

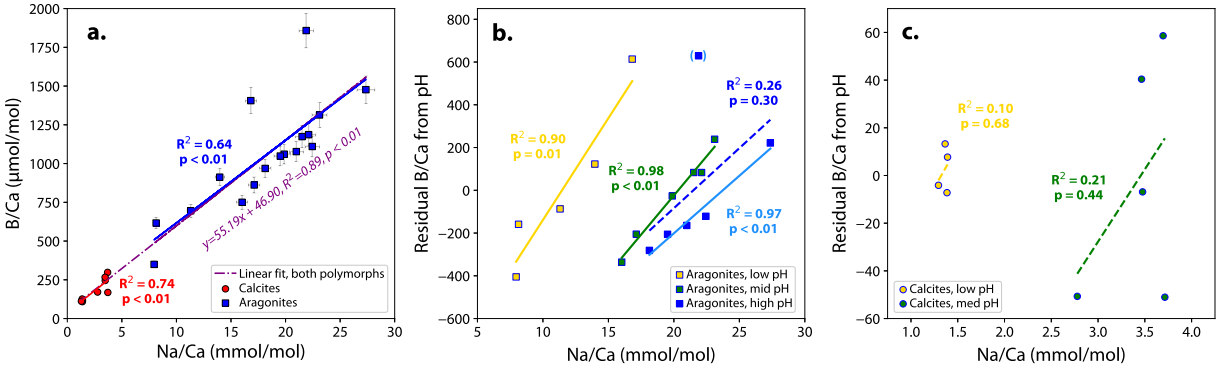

Fig. 4. a) Measured B/Ca vs. Na/Ca ratios in calcites (red circles) and aragonites (blue squares). R-squared values for calcites, aragonites and both polymorphs together are higher than, or comparable to, correlations with any aqueous chemical parameters. Additionally, slopes of linear regressions plotted through either dataset (red and blue lines) are indistinguishable and can be equally well fit with a relationship through both polymorphs (purple line, equation inset). To visualise this another way, in aragonites, as shown in panel b, residual B/Ca around the pH relationship shown in Fig. 2 is strongly correlated with Na/Ca ratios for low and medium pH experiments. At higher pH, an outlier (marked in lighter blue brackets) means that this relationship is not significant (dashed blue line), but when this outlier is removed the relationship between residual B/Ca and Na/Ca is strong for all other datapoints (light blue). For calcites (panel c), the magnitude of residual B/Ca and Na/Ca variability is much lower, and no statistically significant relationships are observed, although regression lines through both low and medium pH calcites are strongly positive, as in aragonites. (For interpretation of the references to colour in this figure legend, the reader is referred to the web version of this article.)

precipitation experiments (Gabitov et al., 2008; Mavromatis et al., 2013), it is similarly difficult to infer anything about precipitation rate in our experiments from this finding.

4.2. Elemental Partitioning: B

We observe a strong carbonate system control on B incorporation into both calcites and aragonites, concordant with the fundamentals of the boron isotope and B/Ca palaeo-proxies, although there is considerable B/Ca variability evident around these relationships (Fig. 3). While we explore any potential aqueous chemical conditions that could have secondarily influenced carbonate B incorporation (Fig. 3), given that within each pH treatment there was relatively little variability in solution chemistry but considerable variability in B/Ca (and Na/Ca), it follows that no obvious correlations arise. Instead, B incorporation exhibits apparently stochastic variability around a predominant carbonate system control within our dataset; variability which is particularly evident in aragonites. This variability, without apparent correlation with any of our (albeit perhaps imperfect) measured growth rate indicators (Fig. 3), would not be expected if incorporation rigidly

follows the surface kinetic model of Branson (2018) with a set rate of attachment and detachment for both aqueous boron species at any given mineralogy and solution chemistry. Indeed, in our dataset, the highest bulk precipitation rates correspond to lower λ_B values (Supp. Fig. 14). It may well be that our experimental carbonates were more highly influenced by the same secondary control on B incorporation that drives the residual unexplained variability in λ_B observed by Farmer et al. (2019), which these authors suggested may be linked to some other control on binding site availability.

One such control on binding site availability, indicated by the close correlation we observed across both calcites and aragonites between Na enrichment and B enrichment (Fig. 4a), and the coherence between residual B/Ca variability and Na/Ca (Fig. 4 b, c) is the provision of B incorporation sites via Na substitution. Na^+ substitutes for Ca^{2+} in calcium carbonate rather than being incorporated at interstitial sites (Yoshimura et al., 2017), and thus a means to maintain charge balance in the crystal lattice is required. Paired incorporation of Na^+ and $B(OH)_4^-$ in place of Ca^{2+} and CO_3^{2-} may be one such mechanism. Indeed, the

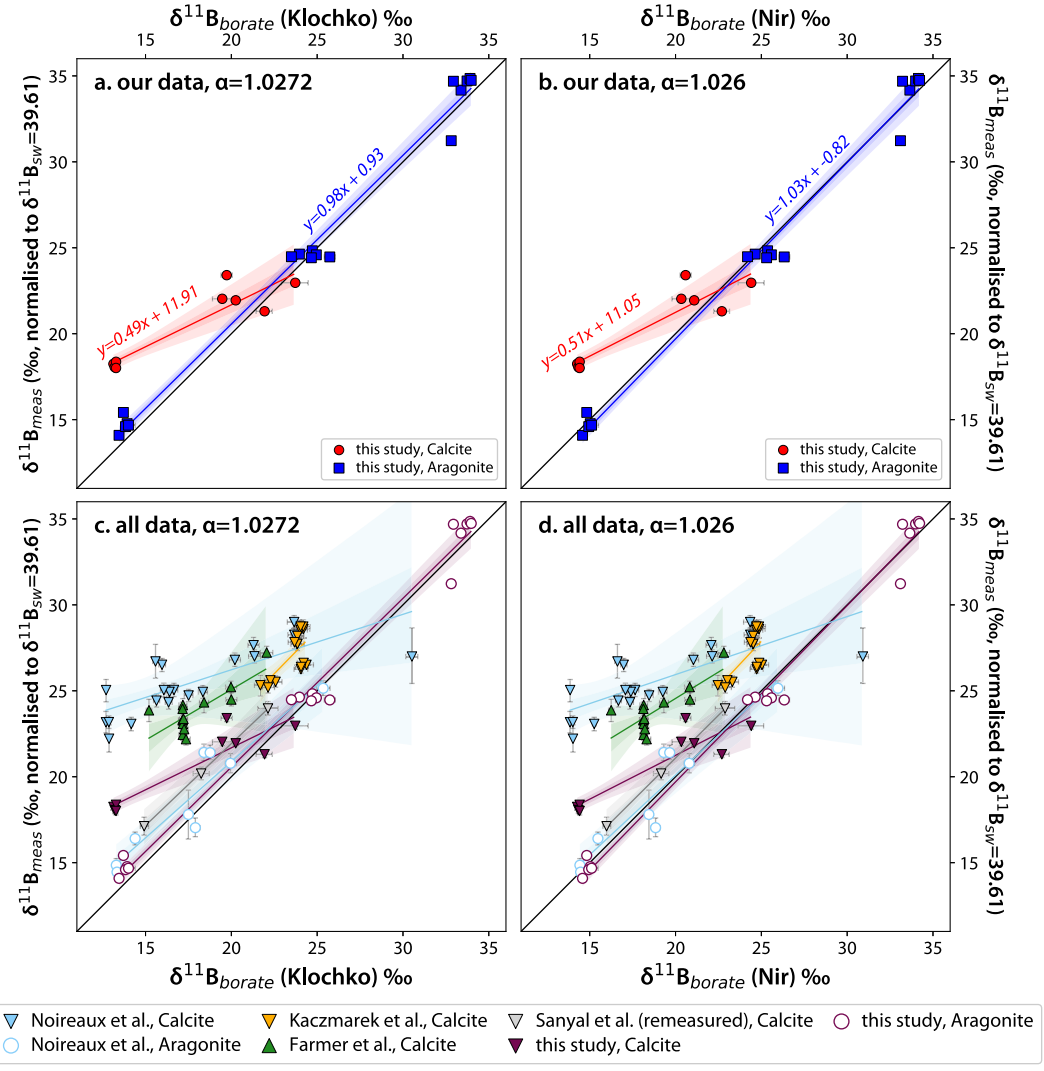

Fig. 5. Boron isotope measurements in calcites (red circles) and aragonites (blue squares) from our study, normalised to a natural seawater value of 39.61 ‰ (Foster et al., 2010) and plotted against $\delta^{11}B_{borate}$ calculated according to an α_B of 1.0272 (panel a; Klochko et al., 2006) and 1.026 (panel b; Nir et al., 2015). In panels c and d, our data (in claret) are shown in the context of data from Noireaux et al. (2015; blue), Kaczmarek et al. (2016; gold) and Farmer et al. (2019; green), as well as the remeasured calcites from Sanyal et al. (2000; grey). Calculated values plotted here use the 'pitzer.dat' database in PHREEQC (Charlton and Parkhurst, 2011b). Error bars on $\delta^{11}B_{carbonate}$ are Monte Carlo propagated 95% confidence intervals, incorporating uncertainty from measurement and uncertainty in experimental fluid $\delta^{11}B$ during the experiment. Error bars on $\delta^{11}B_{borate}$ are Monte Carlo propagated 95 % confidence intervals, incorporating uncertainty from drift in pH and experimental fluid chemistry (and hence pK^*_B) during the experiment. Regression lines plotted, and their 1 and 2 σ confidence intervals (lightly and darkly shaded regions respectively), are constructed using a Monte Carlo 'wild bootstrap' approach (Liu, 1988; Mammen, 1993), where predictor variables are fixed and the regression t-statistic is resampled instead, an approach which is better suited to small datasets (Cameron et al., 2008; Imbens and Kolesar, 2012). (For interpretation of the references to colour in this figure legend, the reader is referred to the web version of this article.)

consistency of this relationship across both carbonate polymorphs, with an intercept close to the origin, suggests that paired incorporation of Na and B may be the primary means by which B can be incorporated into $CaCO_3$ lattice (note, given the order of magnitude greater concentration of Na in $CaCO_3$, it is unlikely to be the other way around). This could also be the basis by which salinity or [Na] enhances B incorporation in inorganic carbonates (Kitano et al., 1978; Uchikawa et al., 2017) and perhaps even biogenic carbonates (Allen et al., 2012). Moreover, if the incorporation of Na into defect sites distorts the $CaCO_3$ lattice structure as it grows (Busenberg and Plummer, 1985), it may follow that Na incorporation is multiplicative, with a more disordered lattice potentially enhancing further substitution of Na^+ for Ca^{2+}, and more $B(OH)_4^-$ with it. In this way, the apparent stochasticity of our B/Ca data in relation to solution chemistry, but their systematic correlation with precipitate Na/Ca, could be explained by differences in the frequency and timing of Na substitution during the nucleation or early growth of experimentally-grown $CaCO_3$, potentially setting the regime for B incorporation thereafter.

4.3. Boron isotope incorporation: aragonite vs calcite

In common with previous studies, we observe relatively poor agreement between the $\delta^{11}B$ of our synthetic calcite and aqueous $\delta^{11}B_{borate}$, considerable scatter between experimental treatments, and a slope (i.e., a pH sensitivity) that is much less than 1 (Fig. 5). In the case of aragonite, however, we observe that $\delta^{11}B_{aragonite}$ closely resembles that of aqueous $\delta^{11}B_{borate}$, confirming the findings of Noireaux et al. (2015) over a wider pH range (~7.4–~9.4). That the relationship between $\delta^{11}B_{aragonite}$ and aqueous $\delta^{11}B_{borate}$ observed here is within uncertainty of that observed by Noireaux et al. (2015) is also significant in itself, since the solution chemistries, ionic strengths, and precipitation techniques used differ considerably between our study and this previous work. For instance, the ionic strength of our solutions was close to mean average seawater (I = 0.7 M), whereas it was considerably lower (I = 0.1–0.2 M) in the experiments of Noireaux et al,. (2015). Therefore, we can conclude that at least in aragonites, solution chemistry appears to have little intrinsic influence on the isotopic partitioning of boron beyond its calculable effect on boron speciation, and that sole incorporation of borate ion, without fractionation during any adsorption step, is strongly implied. With regards the value of α_B, our analyses suggest that an α_B of 1.026 (from Nir et al., 2015) produces a better fit with $\delta^{11}B_{aragonite}$ compared to the α_B of 1.0272 from Klochko et al. (2006). At this stage, we cannot discern whether this supports this later estimate of the fractionation factor between aqueous borate and boric acid as being more accurate (as argued by Noireaux et al. 2015), or whether this is some aragonite-specific fractionation from aqueous borate. In practical terms for the application of the boron isotope-pH proxy, in instances where empirical calibrations are used this should not matter greatly, provided the same value of α_B is used in calibration and reconstruction. However, in cases where a pH-sensitivity equal to aqueous borate is assumed, this should be borne in mind-particularly in the reconstruction of calcification fluid pH from aragonitic coral $\delta^{11}B_{aragonite}$ (e.g. Holcomb et al., 2014; Schoepf et al., 2017).

While the boron isotope composition of our calcite precipitates, as with previous studies, diverges significantly from that calculated for aqueous borate ion, it is notable that our precipitates fall closer to $\delta^{11}B_{borate}$ than other previously published carbonate data (Fig. 5). Indeed, at the upper end of the pH range of our calcite experiments (~8.6), our calcite precipitates record the $\delta^{11}B_{borate}$ more or less faithfully, which speaks against the existence of a universal boron isotope fractionation during adsorption and incorporation at this pH that has been observed elsewhere (Saldi et al., 2018). Possible mechanistic reasons for this are discussed further in the next section, but we suggest that the higher ionic strength of our precipitation solutions may be key. Saldi et al. (2018) observed that the apparent magnitude of fractionation associated with adsorption onto calcite decreased with increasing ionic strength (I), although we note their estimates of the fractionation were also more uncertain with increasing I. We note that proximity in measured $\delta^{11}B$ to aqueous $\delta^{11}B_{borate}$ increases with ionic strength, with our data and those remeasured calcites of Sanyal et al. (2000) – both precipitated at I = ~0.7 mol/kg – closest in measured $\delta^{11}B$ to aqueous borate ion, and Kaczmarek et al. (2016)'s calcite precipitations (I = ~0.6 mol/kg), next closest. Therefore we suggest that isotope fractionation upon adsorption of B onto calcite, while evidently large at low ionic strength (Saldi et al., 2018), is much weaker (and possibly negligible) at ionic strengths typical of seawater conditions. Our data also appear incompatible with the large structural fractionation between aqueous and solid carbonate-hosted B phase advocated by Balan et al. (2016; 2018), perhaps supporting Farmer et al. (2019)'s assessment that simulations at close to thermodynamic equilibrium are likely unrepresentative of conditions at a growing mineral face.

Although the remeasured precipitates of Sanyal et al. (2000), if reliable, show a slope that is much more similar to aqueous borate than when measured via NTIMS (Fig. 5, Supplementary Appendix), and our calcite data in general fall closer to the $\delta^{11}B$ of aqueous borate ion than previous studies, our calcites nonetheless diverge strongly from $\delta^{11}B_{borate}$ at low ambient $\delta^{11}B_{borate}$ (/pH), with a slope considerably less than unity (~0.49–0.51) and considerable scatter (Fig. 5). The offset between measured $\delta^{11}B_{carbonate}$ and aqueous $\delta^{11}B_{borate}$ $\Delta_{C\text{-}B}$ (note we use Δ here rather than ε to avoid confusion with the aqueous fractionation between borate and boric acid, ε_B) in our calcites falls roughly upon the same relationship with SI described by other published data (and as noted by Farmer et al., 2019). Specifically, $\Delta_{C\text{-}B}$ values approach $\delta^{11}B_{borate}$ at high SI, and are increasingly positively offset at low SI (Fig. 6a). According to the SKM model of Branson (2018), the mechanism for this trend is that rates of precipitation are faster than those of detachment of $B(OH)_4^-$ ion from the crystal face at higher SI. Conversely, precipitation rates are lower at low SI, and relatively higher detachment of $B(OH)_4^-$ leaves the bulk crystal relatively enriched in

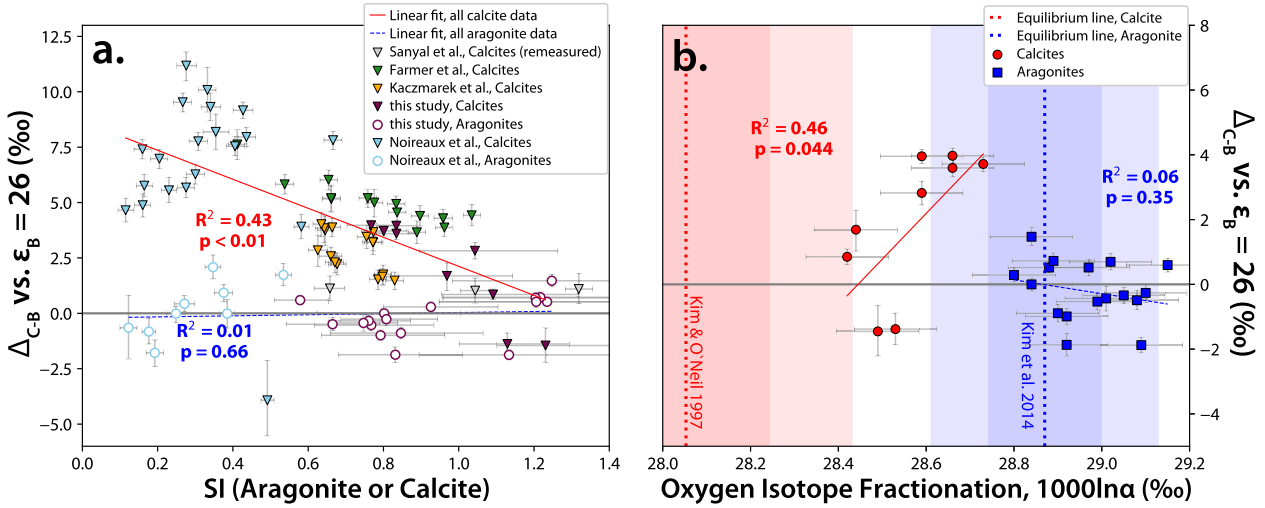

Fig. 6. The offset $\Delta_{C\text{-}B}$ between $\delta^{11}B$ measured in calcite precipitates and the predicted $\delta^{11}B$ of aqueous borate in their experimental growth media (assuming $\varepsilon_B = 26$ ‰, from Nir et al. (2015)) correlates with SI ($R^2 = 0.43$; panel a), which is a common driver of precipitation rate. However, there is considerable scatter in the calcite data from Noireaux et al. (2015) that do not fit this relationship. It may therefore be incorrect to treat SI as a universal proxy for precipitation rate, since in our experiments SI does not correlate well with bulk precipitation rate (Supp. Fig. 4). Furthermore, one might expect the fastest rates of precipitation at high SI, and yet in our study the largest deviations from oxygen isotope equilibrium (panel b), which in the case of calcites also showed the greatest offset from the $\delta^{11}B$ of aqueous borate, were at the lowest SI values. This is inconsistent with increasing $B(OH)_4^-$ incorporation relative to $B(OH)_3$ at high precipitation rates, advocated by Farmer et al. (2019). Data in panel b are plotted in relation to the calcite equilibrium oxygen isotope fractionation of Kim & O'Neil (1997) (red dotted line) and the aragonite equilibrium oxygen isotope fractionation of Kim et al. (2014) (blue dotted line).

trigonal $B(OH)_3$, whose detachment rates are lower. However, as previously discussed, unlike the data of Farmer et al. (2019), SI was if anything negatively correlated with measured bulk precipitation rate in our calcite experiments (see Supp. Fig. 4), and higher bulk precipitation rates in lower pH treatments correspond to the most elevated $\delta^{11}B_{carbonate}$ relative to aqueous $\delta^{11}B_{borate}$. Moreover, if high precipitation rate were the key in trapping $B(OH)_4^-$, one might expect those samples that precipitated furthest from oxygen isotope equilibrium to have the smallest values of $\Delta_{C\text{-}B}$, but if anything those closest to Kim & O'Neil (1997)'s estimate of equilibrium fractionation most closely resemble aqueous $\delta^{11}B_{borate}$ (Fig. 6b). Finally, there are reasons within the dataset of Noireaux et al. (2015) to suspect that rate may not be the primary factor at play: a) the only calcite precipitate from above pH 9 is inconsistent with such a model and b) seeded and unseeded calcites in their experiments showed different surface-area-normalised precipitation rates, and yet this is not reflected in their $\Delta_{C\text{-}B}$.

4.4. Possible reconciliation of disparate findings with surface zeta potential

Although we demonstrate that boron incorporation into aragonite adheres to the established basis of the boron isotope proxy across a wide range of pH, the variability in boron partitioning and isotope fractionation within our calcite data and between published calcite datasets continues to pose a challenge to this paradigm. We suggest, however, that some of this variability might be explicable when one considers the surface coordination environment of the contact solution. For B, Na and Mg to be incorporated into the $CaCO_3$ lattice structure, these ions must first adsorb onto electrostatically-favourable mineral surface sites. The possible exception to this is Mg in aragonite, where adsorption behaviour is not always evident (De Groot and Duyvis, 1966; Mucci and Morse, 1983). Both Na (e.g. Busenberg and Plummer, 1985) and B (Goldberg and Forster, 1991; Saldi et al., 2018; Wang et al., 2018) follow Langmuir adsorption isotherms, suggesting adsorption is the critical first step on the pathway to their incorporation. Typically, sorption reactions are discussed in relation to a mineral's surface charge. In the case of most metal oxides surface charge is determined by the relative concentrations of H^+ and OH^- ions (the 'potential determining ions', or PDIs) in solution (e.g. Schindler and Stumm, 1987), and thus it is pH dependent. However, surface electrostatic behaviour of $CaCO_3$ is more complex, as free Ca^{2+} and CO_3^{2-} ions (whose speciation itself may be pH dependent) are instead the principle PDIs (Foxall et al., 1979). Indeed, as summarised by Al Mahrouqi et al. (2017), varying pH while keeping pCa constant will not change the electrostatic behaviour of calcite. This, coupled with the solubility of $CaCO_3$ in water and the fact that one of the PDIs, CO_3^{2-}, is also sensitive to equilibration with the atmosphere, has meant that published measurements of $CaCO_3$ surface potential have often been inconsistent (see Wolthers et al., 2008; Al Mahrouqi et al., 2017 for a summary).

Additionally, unlike in the case of metal oxides, the effective surface charge of $CaCO_3$ in water is not in itself sensitive to pH: a well-ordered water layer exists at the interface of the mineral (Fenter et al., 2000; Fenter and Sturchio, 2004; Geissbühler et al., 2004), termed the hydrolysis layer (Stipp, 1999) or 0-plane (Heberling et al., 2011),

and at this plane the charge should be weakly negative across a wide range of pH (5.5–11; Heberling et al., 2011). The parameter that controls an affinity of the carbonate surface for dissolved anions or cations in the bulk solution is therefore not the surface charge of the terminal edge of the mineral lattice, as is often discussed (e.g. Branson, 2018; Saldi et al., 2018), but the zeta potential (ζ-potential), which is defined as the electrostatic potential at the outer Helmholtz plane (OHP; the outermost plane of the Stern layer, where strongly bonded hydrated cations reside in fixed-positions coordinated with the terminal edge, see Fig. 7 for a schematic). Between the Stern layer and the bulk solution (where potential = 0 mV) lies the diffuse layer, where anions and cations are mobile, and will be repelled or attracted to the OHP according to their charge. Together, the hydrolysis layer, Stern layer (including inner and outer Helmholtz planes) and diffuse layer make up the 'electric double layer' or EDL (see helpful summaries in Stipp, 1999; Al Mahrouqi et al., 2017). When viewed within this framework, the steps which an ion must go through to be incorporated in the solid phase are: (a) migration through the potential gradient in the diffuse layer, (b) adsorption at, and lateral migration along, the Stern layer, and (c) removal of the chemi-sorbed OH^- and H^+ at the termination of the mineral lattice in the hydrolysis plane such that the ion can finally meet its binding site and coprecipitate. Solution chemistry will likely have effects on all of these steps, but we particularly focus on the first two here.

Considering the observed ζ-potential of a growing carbonate mineral, which is weakly negative in most natural settings (e.g. Berlin and Khabakov, 1961; Cicerone et al., 1992; Al Mahrouqi et al., 2017), rather than charge at the terminal layer of the crystal, which is typically considered to be positive (e.g. Kitano et al., 1978; Branson, 2018), the attraction and adsorption of only tetrahedrally coordinated B (i.e. $B(OH)_4^-$) to carbonate minerals becomes more difficult to explain. One potential route for $B(OH)_4^-$ (and not $B(OH)_3$; Saldi et al. (2018)) to migrate against a gradient in electrostatic potential and adsorb at the Stern layer could be attraction as part of a complex with aqueous Ca^{2+} ($CaB(OH)_4^+$) or Mg^{2+} ($MgB(OH)_4^+$). These complexes can host up to 19 % of the dissolved tetrahedral $B(OH)_4^-$ within the experimental solutions examined here, as calculated using the pitzer.dat database, suggesting this is not unreasonable. Such a mechanism might also help to explain the decrease in $B(OH)_4^-$ adsorption to the calcite surface at high pH (Saldi et al., 2018), despite ζ-potential likely remaining similarly negative at higher pH, since at high pH much less $B(OH)_4^-$ ion is complexed with Ca^{2+} or Mg^{2+} in relative terms. Uncharged $NaB(OH)_4$ ion pairs might also provide a vector for $B(OH)_4^-$ to cross this electrostatic gradient, with this ion pair either then being incorporated together by paired substitution or dissociated at the Stern layer.

In the absence of other influences, the concentrations of the main PDIs (Ca^{2+} and CO_3^{2-}) in a solution will affect the magnitude (and perhaps sign) of the ζ-potential, by altering the coverage density of PDIs at the Stern layer. At higher concentrations of Ca^{2+}, i.e. lower pCa, ζ-potential in carbonates gets progressively more positive (Al Mahrouqi et al., 2017), thereby reducing the potential energy needed to bring a negatively-charged ion to the OHP. Other ions in solution may also act as PDIs. Although Ca^{2+} and CO_3^{2-} are the primary PDIs, Mg^{2+} is thought to also affect calcite ζ-potential almost, or just as strongly as Ca^{2+} (Cicerone et al., 1992; Al Mahrouqi et al., 2017), and even Na^+, often considered an indifferent ion, may act as a PDI in some settings (Al Mahrouqi et al., 2017). Others have observed that PO_4^{3-} in solution, which has been shown to influence B incorporation (Henehan et al., 2015; Uchikawa et al., 2017), also lowers calcite ζ-potential (Douglas and Walker, 1950; Amankonah and Somasundaran, 1985). In the case of published boron-carbonate coprecipitations, most studies (ours included) have attempted to maintain roughly constant saturation (and hence precipitation rate) at low pH by compensating

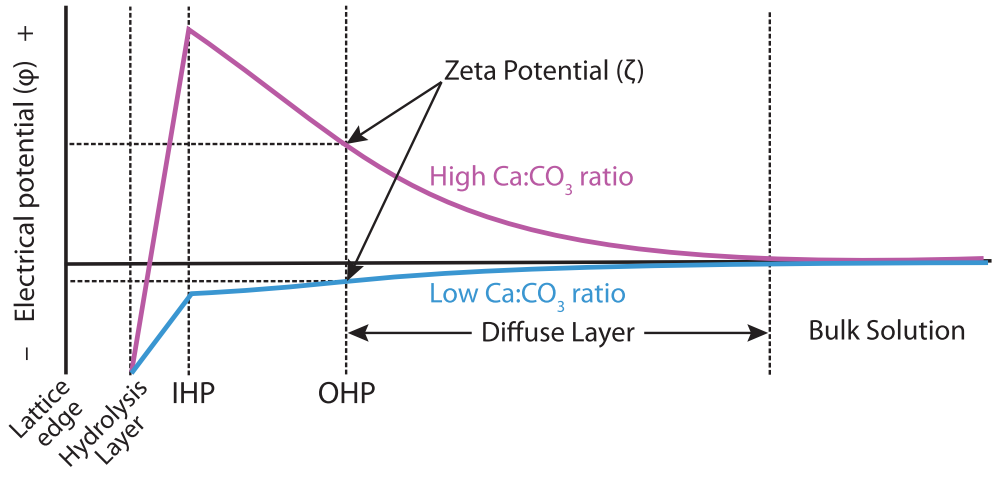

Fig. 7. Schematic representation of electrostatics at the mineral face, from the first hydrolysis layer (Heberling et al., 2011), through the inner Helmholtz plane (IHP; where ions are specifically adsorbed to the mineral face), outer Helmholtz plane (OHP; where ions are non-specifically adsorbed, retaining their hydration shell), and diffuse layer, where ions are electrostatically attracted to or repulsed by the charge at the OHP (i.e. the zeta potential), but can move around. The ratio of potential-determining ions (PDIs) Ca^{2+} and CO_3^{2-} will alter the zeta potential.

for the lack of aqueous CO_3^{2-} ion with increases in $[Ca^{2+}]$. Although this keeps Ω roughly constant, by altering the ratio of these important PDIs, the resultant changes in ζ-potential (and hence the ease at which positive vs. negative ions reach the OHP surface) are likely much larger than would ever be seen in natural systems. With this in mind, plotting the residuals from the relationship between experimental calcite $\Delta_{C\text{-}B}$ and SI (Fig. 8a) against the ratio of the key PDIs in solution yields a strong correlation (Fig. 8b), suggesting that the ratio of PDIs plays a parallel role in influencing boron incorporation, and may well be the unknown secondary control hinted at by Farmer et al. (2019). Together, SI and the ratio of PDIs can explain 73 % of the variability in $\Delta_{C\text{-}B}$ seen in experimental calcites to date (Fig. 8c), although we note that factors other than the ratio of these two PDIs can influence ζ-potential, and as such it may be that electrostatics play a role in explaining the other 27 % of observed variance. Promisingly, the PDI ratio can explain much of the variability in the calcites of Noireaux et al. (2015) that are otherwise poorly explained (Fig. 6) by an SI or precipitation rate-driven scenario (Farmer et al., 2019), without needing to discount any data points as outliers. That these data should be the most influenced by PDI ratio is consistent with expectations from the electric double layer, because ionic strength in solution determines the thickness of the diffuse layer (essentially because at higher ionic strengths there are more charged ions contained within the diffuse layer with which charge can be balanced). Generally speaking, this means that at higher ionic strengths, the ζ-potential of $CaCO_3$ is closer to zero, and is less easily perturbed by other experimental parameters (e.g. Glover et al., 2012; Al Mahrouqi et al., 2016). Thus, the effect of changes in experimental conditions on ζ-potential are likely to be much greater for lower ionic strength experiments such as Noireaux et al. (2015)'s ($I = 0.1$–0.2 M), than for conditions closer to seawater. This phenomenon is further evidenced in the experiments of Saldi et al. (2018), where the amplitude of change in boron adsorption with carbonate system change was progressively dampened with higher ionic strength - consistent with a collapsing of the diffuse layer.

One other experimental parameter that may influence the ζ-potential of $CaCO_3$ is the amount of mineral surface relative to experimental solution, with observed ζ-potential varying with specific surface area (e.g. Vdović, 2001). As boron and other impurities will produce more surface roughness on a growing crystal face (Dove et al., 2004; Ruiz-Agudo et al., 2012), as well as altering its surface charge (notwithstanding possible compensation in the hydrolysis plane), it is therefore conceivable that positive feedbacks might emerge between incorporation of impurities and changing ζ-potential, thus accentuating stochastic variation in element partitioning, and perhaps isotope fractionation. Relatedly, the concentration of solid grains in an experimental solution – which varies considerably between and within the experiments examined here – may also affect ζ-potential, with increasing solid–liquid ratios making ζ-potential more positive (Siffert and Fimbel, 1984; Vdović, 2001; Wang et al., 2018), and more so in calcites than aragonites (Wang et al., 2018), although it is unclear if all such observations are at equilibrium pCa (Al Mahrouqi et al., 2017). While we see no correlation between particle density (in mg/L) and residual variability around our multivariate model, we highlight this issue for consideration when designing future precipitation experiments.

Considerations of ζ-potential may also help to explain the differences observed to date in boron co-precipitation behaviour between natural and synthetic calcites. Synthetic calcites show consistently more variable ζ-potential than natural or biogenic calcites (Al Mahrouqi et al., 2017, and references within), and may be positive or negative. Biogenic calcites, however, display (with few documented exceptions) weakly negative ζ-potential, probably as a result of the presence of organic components (Cicerone

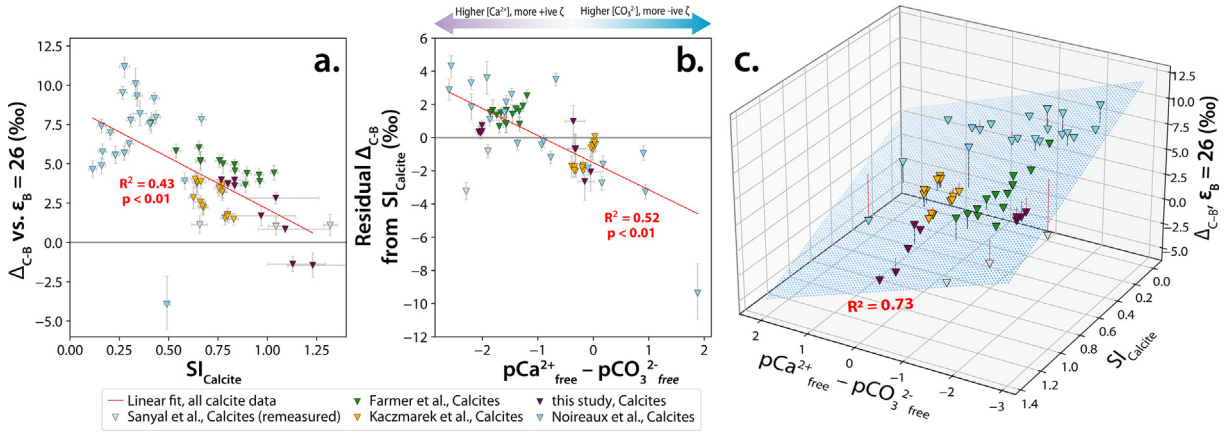

Fig. 8. $\Delta_{C\text{-}B}$ – the offset between measured $\delta^{11}B$ in calcite precipitates and predicted $\delta^{11}B$ of aqueous borate (calculated at ε_B,= 26 ‰) – correlates reasonably well with SI, as seen in other studies (panel a), although there is significant unexplained variability – particularly visible in the data of Noireaux et al. (2015). Plotting the residuals from this relationship the ratio of PDIs in solutions, however, can explain the majority of this residual variability (panel b)- suggesting that variable ζ-potential in experimental setups may play a role in explaining observed patterns. With these two variables alone, 73 % of the variance in $\Delta_{C\text{-}B}$ can be explained (panel c). See electronic supplement for animated version of panel c.

et al., 1992; Vdović, 2001). This more controlled, consistently negative ζ-potential might help to explain less variable boron partitioning and isotope fractionation observed in biogenic calcite (at least within a species) as compared to the considerable scatter seen in synthetic calcites.

While patterns in our and others' inorganic precipitate measurements suggest electrostatic controls on B adsorption could be a promising avenue of future research, since our experiments were not designed with this in mind, we cannot put forward a more complete framework for how this would induce the observed variability in $\delta^{11}B$ in synthetic carbonates at this stage. However, we propose two possible models that may merit future examination. Firstly, Saldi et al. (2018) note that strong electrostatic effects within the EDL could alter the equilibrium isotopic fractionation of aqueous boron through the Stark effect (Lambert, 1996), modifying the vibrational frequencies of the adsorbed borate relative to the free borate ion. Via this scenario, stronger and more variable polarity ζ-potential in low ionic strength solutions could explain the larger and more variable values of $\Delta_{C\text{-}B}$ seen by Noireaux et al. (2015) compared to other studies, and the relatively weaker fractionation upon adsorption with ionic strength observed by Saldi et al. (2018). Observed differences in $\delta^{11}B$ between aragonite and calcite – with aragonite appearing to record aqueous borate assuming Nir et al. (2015)'s aqueous fractionation factor of 1.026 across a range of ionic strengths, but calcite diverging – could then be explained by relatively weaker electrostatic forces (and correspondingly less sensitivity to ionic strength) at the face of the aragonite polymorph. Although the vast majority of published investigations into ζ-potential are motivated by industrial applications and thus have focussed on calcites, limited comparisons within broader studies do suggest aragonites and calcites show different ζ-potential responses to solution chemistry (De Groot and Duyvis, 1966; Smallwood, 1977; Moulin and Roques, 2003), indicating this may be a fruitful avenue of investigation.

A second, alternative scenario, involves isotopic fractionation not associated with adsorption or re-coordination of B, as is often considered (Balan et al., 2018; Saldi et al., 2018; Farmer et al., 2019), but upon detachment of $B(OH)_4^-$ from the growing crystal surface. If the ζ-potential of calcite is weakly negative under more natural distributions of PDIs, $B(OH)_4^-$ is unlikely to be electrostatically attracted to the Stern layer – and hence the growing calcite face – unless it crosses the gradient in potential in the diffuse layer as a positively charged ion pair as $CaB(OH)_4^+$ or $MgB(OH)_4^+$. These aqueous ion pairs at equilibrium are not thought to be strongly isotopically distinct from the free aqueous borate pool (Saldi et al., 2018). However, it is conceivable that they may enhance the likelihood of kinetic isotope fractionation if within the pool of e.g. $CaB(OH)_4^+$, $Ca^{11}B(OH)_4^+$ bonds are stronger or slower to break than those of $Ca^{10}B(OH)_4^+$. If, while moving laterally through the Stern layer, a paired Ca^{2+} ion successfully makes contact with the termination of the crystal lattice, charge balance considerations mean its paired $B(OH)_4^-$ is an obstacle to incorporation. Thus either 1) the Ca^{2+}-$B(OH)_4^-$ association must be broken, 2) the $CaB(OH)_4^+$ pair must be detached, or 3) this boron is facilitated in the lattice, either by paired incorporation of a monovalent cation (e.g. Na^+) to maintain local charge balance, or by propagation of defects in the lattice structure. If $Ca^{11}B(OH)_4^+$ associations are harder (or slower) to break than $Ca^{10}B(OH)_4^+$, then the heavier $Ca^{11}B(OH)_4^+$ pair is more likely to be retained long enough for either a compensating monovalent cation to arrive or for the lattice to grow around the new defect. By this model, negative ζ-potential (and potentially higher ionic strength) would mean more likelihood of Na^+ being attracted to the Stern layer in sufficient quantity to remove the need for $B(OH)_4^-$ detachment (and hence fractionation). Conversely, at low pCa (more positive ζ-potential), strong attraction for the divalent negative CO_3^{2-} may result in relative exclusion of Na^+ ions close to the shear plane (and thus a greater propensity for kinetic fractionation due to differential detachment rates) and perhaps a faster rate of entrapment at the lattice front. Difference in behaviour between calcite and aragonite could then be explained by either a) more consistently negative ζ-potential in aragonite, or b) a lattice structure that is more accommodating of one or both of Na^+ and $B(OH)_4^-$. Furthermore, precipitation rate effects could also be accommodated by this model, with faster crystal growth rates meaning a greater likelihood that adsorbed $B(OH)_4^-$ is incorporated before detachment can occur.

5. CONCLUSIONS: IMPLICATIONS FOR STUDY OF BIOGENIC CARBONATES AND THE BORON ISOTOPE-PH PROXY

In this study, we present new $\delta^{11}B$ measurements of synthetic calcites and aragonites, precipitated in the presence of Mg and at approximately seawater-like ionic strength (~0.7 mol/kg). B incorporation in both polymorphs increases with solution pH, although with considerable variability in B/Ca within similar experimental treatments, particularly in aragonites. However, a tight correlation between measured B/Ca and Na/Ca, consistent across both polymorphs, may indicate an important link between Na and B incorporation at the crystal surface. Although we cannot rule out the possibility that none of our metrics of precipitation rate (Fig. 3, Supp Fig. 3) reflect surface area-normalised growth rates at the mineral-fluid interface, we see no strong correlation between precipitation rate and boron partitioning or isotopic fractionation compared to aqueous borate ion, unlike in previous work (e.g. Farmer et al., 2019). Our aragonite precipitates – precipitated at or close to predicted oxygen isotope equilibrium (Kim et al. 2014) – support the conclusion of Noireaux et al. (2015) that aragonite records the $\delta^{11}B$ of aqueous borate with negligible fractionation, supporting the use of the boron isotope proxy in e.g. corals for constraining calcifying fluid carbonate chemistry (e.g. McCulloch et al., 2018). In addition, we find that a value of α_B of 1.026 (Nir et al., 2015) is more appropriate for use, at least in aragonite. Contrastingly, while our calcite precipitates (and those of Sanyal et al. (2000), remeasured by MC-ICPMS) are closer in $\delta^{11}B$ to borate ion than some previous

studies, they still show considerable scatter and are increasingly removed from $\delta^{11}B_{borate}$ at low pH. While at face value this might throw doubt on the application of the proxy in uncalibrated calcites to reconstruct ambient pH, it may be that inorganic precipitation experiments such as these may not be representative of natural conditions. Specifically, experimental designs during precipitation of synthetic calcites have likely driven variable ζ-potentials that are unrepresentative of those seen in biogenic calcites. We put forward two mechanisms by which anomalous patterns could be driven by adsorption electrostatics: either due to the Stark vibrational effect (as suggested by Saldi et al., 2018), or as a result of cation-B pairs exacerbating normally weak kinetic isotope effects. This latter mechanism could also play a role in explaining precipitation rate effects at a constant ζ-potential. While surface complexation modelling, ab initio calculations and precipitation experiments incorporating ζ-potential measurements beyond the scope of this study are required, our data nonetheless advance our understanding of boron incorporation pathways in calcium carbonate, and highlight the importance when addressing this question of considering multiple (possibly interacting) ions, rather than focussing on boron in isolation. In particular, we suggest the provision of binding sites for $B(OH)_4^-$ by Na^+ substitution for Ca^{2+} in the $CaCO_3$ lattice warrants further investigation.

Declaration of Competing Interest

The authors declare that they have no known competing financial interests or personal relationships that could have appeared to influence the work reported in this paper.

ACKNOWLEDGEMENTS

We thank Oscar Branson, Jesse Farmer and Joji Uchikawa for their helpful and open discussions throughout the drafting of this manuscript, and in particular Oscar Branson for assistance in implementing pitzer calculations via PHREEQCpy. We also thank Roberts Blukis for helpful discussion, Oded Nir, Yongliang Xiong and David Parkhurst for helpful insights in calculating aqueous chemical speciation, and Vasileios Mavromatis and Jelle Bijma for providing further information about previously published data. We are grateful for the editorial handling of associate editor Marietta Wolthers, and for helpful, insightful and constructive reviews from David Evans and two anonymous reviewers. The B-Team (in particular Joseph Stewart), Andy Milton, Matthew Cooper and Agnes Michalik at the University of Southampton are thanked for their help during these analyses. This research was supported by American Chemical Society – Petroleum Research Fund (ACS-PRF #50755-ND2), Natural Science and Engineering Research Council (NSERC) - Discovery Grants Program (386188-2010), Ontario Ministry of Research and Innovation - Ontario Research Fund (MRI-ORF #28001), Canada Foundation for Innovation - Leaders Opportunity Fund (CFI-LOF #28001) to S.-T. Kim

APPENDIX A. SUPPLEMENTARY MATERIAL

Supplementary data to this article can be found online at https://doi.org/10.1016/j.gca.2021.12.011.

REFERENCES

Al M. D., Vinogradov J. and Jackson M. D. (2016) Temperature dependence of the zeta potential in intact natural carbonates. *Geophys. Res. Lett.* **43**, 11578–11587.

Al M. D., Vinogradov J. and Jackson M. D. (2017) Zeta potential of artificial and natural calcite in aqueous solution. *Adv. Colloid Interface Sci.* **240**, 60–76.

Allen K. A. and Hönisch B. (2012) The planktic foraminiferal B/Ca proxy for seawater carbonate chemistry: A critical evaluation. *Earth Planet. Sci. Lett.* **345–348**, 203–211.

Allen K. A., Hönisch B., Eggins S. M. and Rosenthal Y. (2012) Environmental controls on B/Ca in calcite tests of the tropical planktic foraminifer species Globigerinoides ruber and Globigerinoides sacculifer. *Earth Planet. Sci. Lett.* **351–352**, 270–280.

Amankonah J. O. and Somasundaran P. (1985) Effects of dissolved mineral species on the electrokinetic behavior of calcite and apatite. *Colloids Surf.* **15**, 335–353.

Anagnostou E., John E. H., Edgar K. M., Foster G. L., Ridgwell A., Inglis G. N., Pancost R. D., Lunt D. J. and Pearson P. N. (2016) Changing atmospheric CO_2 concentration was the primary driver of early Cenozoic climate. *Nature* **533**, 380–384.

Babila T. L., Penman D. E., Hönisch B., Kelly D. C., Bralower T. J., Rosenthal Y. and Zachos J. C. (2018) Capturing the global signature of surface ocean acidification during the Palaeocene-Eocene Thermal Maximum. *Philos. Trans. R. Soc. Math. Phys. Eng. Sci.* **376**, 20170072.

Balan E., Noireaux J., Mavromatis V., Saldi G. D., Montouillout V., Blanchard M., Pietrucci F., Gervais C., Rustad J. R., Schott J. and Gaillardet J. (2018) Theoretical isotopic fractionation between structural boron in carbonates and aqueous boric acid and borate ion. *Geochim. Cosmochim. Acta* **222**, 117–129.

Balan E., Pietrucci F., Gervais C., Blanchard M., Schott J. and Gaillardet J. (2016) First-principles study of boron speciation in calcite and aragonite. *Geochim. Cosmochim. Acta* **193**, 119–131.

Berlin T. S. and Khabakov A. V. (1961) Differences in the electrokinetic potential of carbonate sedimentary rocks of different origin and composition. *Geochemistry* **3**, 217–230.

Berner R. A. (1975) The role of magnesium in the crystal growth of calcite and aragonite from sea water. *Geochim. Cosmochim. Acta* **39**, 489–504.

Branson O. (2018) Boron Incorporation into Marine CaCO3. In *Boron Isotopes* (eds. H. Marschall and G. Foster). Springer International Publishing, Cham. pp. 71–105. Available at: http://link.springer.com/10.1007/978-3-319-64666-4_4 [Accessed April 10, 2018].

Branson O., Kaczmarek K., Redfern S. A. T., Misra S., Langer G., Tyliszczak T., Bijma J. and Elderfield H. (2015) The coordination and distribution of B in foraminiferal calcite. *Earth Planet. Sci. Lett.* **416**, 67–72.

Busenberg E. and Plummer L. N. (1985) Kinetic and thermodynamic factors controlling the distribution of SO_4^{2-} and Na^+ in calcites and selected aragonites. *Geochim. Cosmochim. Acta* **49**, 713–725.

Cameron A. C., Gelbach J. B. and Miller D. L. (2008) Bootstrap-Based Improvements for Inference with Clustered Errors. *Rev. Econ. Stat.* **90**, 414–427.

Chalk T. B., Hain M. P., Foster G. L., Rohling E. J., Sexton P. F., Badger M. P. S., Cherry S. G., Hasenfratz A. P., Haug G. H., Jaccard S. L., Martínez-García A., Pälike H., Pancost R. D. and Wilson P. A. (2017) Causes of ice age intensification across the Mid-Pleistocene Transition. *Proc. Natl. Acad. Sci.* **114**, 13114–13119.

Charlton S. R. and Parkhurst D. L. (2011) Modules based on the geochemical model PHREEQC for use in scripting and programming languages. *Comput. Geosci.* **37**, 1653–1663.

Cicerone D. S., Regazzoni A. E. and Blesa M. A. (1992) Electrokinetic properties of the calcite/water interface in the presence of magnesium and organic matter. *J. Colloid Interface Sci.* **154**, 423–433.

Cusack M., Kamenos N. A., Rollion-Bard C. and Tricot G. (2015) Red coralline algae assessed as marine pH proxies using 11B MAS NMR. *Sci. Rep.* **5**, 8175. Available at: http://www.nature.com/articles/srep08175 [Accessed April 10, 2018].

Davies C. W. (1938) 397. The extent of dissociation of salts in water. Part VIII. An equation for the mean ionic activity coefficient of an electrolyte in water, and a revision of the dissociation constants of some sulphates. *J. Chem. Soc.*, 2093.

De Groot K. and Duyvis E. M. (1966) Crystal Form of Precipitated Calcium Carbonate as influenced by Adsorbed Magnesium Ions. *Nature* **212**, 183–184.

DePaolo D. J. (2011) Surface kinetic model for isotopic and trace element fractionation during precipitation of calcite from aqueous solutions. *Geochim. Cosmochim. Acta* **75**, 1039–1056.

Dickson A. G. (1990a) Oceanographic Research Papers : Thermodynamics of the dissociation of boric acid in synthetic seawater from 273.15 to 318.15 K. *Deep Sea Res. Part A* **37**, 755–766.

Dickson A. G. (1990b) Thermodynamics of the dissociation of boric acid in potassium chloride solutions from 273.15 to 318.15 K. *J. Chem. Eng. Data* **35**, 253–257.

Douglas H. W. and Walker R. A. (1950) The electrokinetic behaviour of Iceland spar against aqueous electrolyte solutions. *Trans. Faraday Soc.* **46**, 559.

Dove P. M., de Yoreo J. J. and Davis K. J. (2004) Inhibition of $CaCO_3$ crystallization by small molecules: the magnesium example. In *Nannoscale structure and assembly at solid-fluid interfaces, volume II: Assembly in Hybrid and Biological Systems Kluwer Academic Publishers*. Dordecht, Netherlands, pp. 56–82.

Epstein S. and Mayeda T. (1953) Variation of O^{18} content of waters from natural sources. *Geochim. Cosmochim. Acta* **4**, 213–224.

Evans D., Gray W. R., Rae J. W. B., Greenop R., Webb P. B., Penkman K., Kröger R. and Allison N. (2020) Trace and major element incorporation into amorphous calcium carbonate (ACC) precipitated from seawater. *Geochim. Cosmochim. Acta* **290**, 293–311.

Farmer J. R., Branson O., Uchikawa J., Penman D. E., Hönisch B. and Zeebe R. E. (2019) Boric acid and borate incorporation in inorganic calcite inferred from B/Ca, boron isotopes and surface kinetic modeling. *Geochim. Cosmochim. Acta* **244**, 229–247.

Farmer J. R., Hönisch B. and Uchikawa J. (2016) Single laboratory comparison of MC-ICP-MS and N-TIMS boron isotope analyses in marine carbonates. *Chem. Geol.* **447**, 173–182.

Fenter P., Geissbühler P., DiMasi E., Srajer G., Sorensen L. B. and Sturchio N. C. (2000) Surface speciation of calcite observed in situ by high-resolution X-ray reflectivity. *Geochim. Cosmochim. Acta* **64**, 1221–1228.

Fenter P. and Sturchio N. C. (2004) Mineral–water interfacial structures revealed by synchrotron X-ray scattering. *Prog. Surf. Sci.* **77**, 171–258.

Foster G. L. (2008) Seawater pH, pCO_2 and $[CO_3^{2-}]$ variations in the Caribbean Sea over the last 130kyr: A boron isotope and B/Ca study of planktic foraminifera. *Earth Planet. Sci. Lett.* **271**, 254–266.

Foster G. L., Hönisch B., Paris G., Dwyer G. S., Rae J. W. B., Elliott T. R., Gaillardet J., Hemming N. G., Louvat P. and Vengosh A. (2013) Interlaboratory comparison of boron isotope analyses of boric acid, seawater and marine $CaCO_3$ by MC-ICPMS and NTIMS. *Chem. Geol.* **358**, 1–14.

Foster G. L. and Rae J. W. B. (2016) Reconstructing Ocean pH with Boron Isotopes in Foraminifera. *Annu. Rev. Earth Planet. Sci.* **44**, 207–237.

Foster G. L., Strandmann P. A. E. P. von and Rae J. W. B. (2010) Boron and magnesium isotopic composition of seawater. *Geochem. Geophys. Geosystems* **11**, Q08015.

Foxall T., Peterson G. C., Rendall H. M. and Smith A. L. (1979) Charge determination at calcium salt/aqueous solution interface. *J. Chem. Soc. Faraday Trans. 1 Phys. Chem. Condens. Phases* **75**, 1034.

Füger A., Konrad F., Leis A., Dietzel M. and Mavromatis V. (2019) Effect of growth rate and pH on lithium incorporation in calcite. *Geochim. Cosmochim. Acta* **248**, 14–24.

Furst M., Lowenstam H. A. and Burnett D. S. (1976) Radiographic study of the distribution of boron in recent mollusc shells. *Geochim. Cosmochim. Acta* **40**, 1381–1386.

Gabitov R. I., Gaetani G. A., Watson E. B., Cohen A. L. and Ehrlich H. L. (2008) Experimental determination of growth rate effect on U^{6+} and Mg^{2+} partitioning between aragonite and fluid at elevated U^{6+} concentration. *Geochim. Cosmochim. Acta* **72**, 4058–4068.

Gagnon A. C., Gothmann A. M., Branson O., Rae J. W. B. and Stewart J. A. (2021) Controls on boron isotopes in a cold-water coral and the cost of resilience to ocean acidification. *Earth Planet. Sci. Lett.* **554** 116662.

Geissbühler P., Fenter P., DiMasi E., Srajer G., Sorensen L. B. and Sturchio N. C. (2004) Three-dimensional structure of the calcite–water interface by surface X-ray scattering. *Surf. Sci.* **573**, 191–203.

Glover P. W. J., Walker E. and Jackson M. D. (2012) Streaming-potential coefficient of reservoir rock: A theoretical model. *Geophysics* **77**, D17–D43.

Goldberg S. and Forster H. S. (1991) Boron sorption on calcareous soils and reference calcites. *Soil Sci.* **152**, 304–310.

Hain M. P., Sigman D. M., Higgins J. A. and Haug G. H. (2015) The effects of secular calcium and magnesium concentration changes on the thermodynamics of seawater acid/base chemistry: Implications for Eocene and Cretaceous ocean carbon chemistry and buffering. *Glob. Biogeochem. Cycles* **29**(5), 517–533.

Heberling F., Trainor T. P., Lützenkirchen J., Eng P., Denecke M. A. and Bosbach D. (2011) Structure and reactivity of the calcite–water interface. *J. Colloid Interface Sci.* **354**, 843–857.

Hemming N. G. and Hanson G. N. (1992) Boron isotopic composition and concentration in modern marine carbonates. *Geochim. Cosmochim. Acta* **56**, 537–543.

Henehan M. J., Edgar K. M., Foster G. L., Penman D. E., Hull P. M., Greenop R., Anagnostou E. and Pearson P. N. (2020) Revisiting the Middle Eocene Climatic Optimum 'Carbon Cycle Conundrum' with new estimates of atmospheric pCO_2 from boron isotopes. *Paleoceanogr. Paleoclimatol.* **35**.

Henehan M. J., Foster G. L., Rae J. W. B., Prentice K. C., Erez J., Bostock H. C., Marshall B. J. and Wilson P. A. (2015) Evaluating the utility of B/Ca ratios in planktic foraminifera as a proxy for the carbonate system: A case study of *Globigerinoides ruber*: Investigating controls on *G. ruber* B/Ca. *Geochem. Geophys. Geosystems* **16**, 1052–1069.

Henehan M. J., Rae J. W. B., Foster G. L., Erez J., Prentice K. C., Kucera M., Bostock H. C., Martínez-Botí M. A., Milton J. A., Wilson P. A., Marshall B. J. and Elliott T. (2013) Calibration of the boron isotope proxy in the planktonic foraminifera *Globigerinoides ruber* for use in palaeo-CO_2 reconstruction. *Earth Planet. Sci. Lett.* **364**, 111–122.

Hershey J. P., Fernandez M., Milne P. J. and Millero F. J. (1986) The ionization of boric acid in NaCl, Na-Ca-Cl and Na-Mg-Cl solutions at 25°C. *Geochim. Cosmochim. Acta* **50**, 143–148.

Holcomb M., DeCarlo T. M., Gaetani G. A. and McCulloch M. (2016) Factors affecting B/Ca ratios in synthetic aragonite. *Chem. Geol.* **437**, 67–76.

Holcomb M., Venn A. A., Tambutté E., Tambutté S., Allemand D., Trotter J. and McCulloch M. (2014) Coral calcifying fluid pH dictates response to ocean acidification. *Sci. Rep.* **4**, 5207. Available at: http://www.nature.com/articles/srep05207 [Accessed May 4, 2020].

Hönisch B., Bijma J., Russell A. D., Spero H. J., Palmer M. R., Zeebe R. E. and Eisenhauer A. (2003) The influence of symbiont photosynthesis on the boron isotopic composition of foraminifera shells. *Mar. Micropaleontol.* **49**, 87–96.

Hönisch B., Eggins S., Haynes L. L., Allen K. A., Holland K. D. and Lorbacher K. (2019) *Boron proxies in paleoceanography and paleoclimatology*. Wiley Blackwell, Hoboken, NJ.

Imbens G. W. and Kolesar M. (2012) *Robust Standard Errors in Small Samples: Some Practical Advice.*, National Bureau of Economic Research. Available at: http://www.nber.org/papers/w18478 [Accessed January 24, 2016].

Kaczmarek K., Nehrke G., Misra S., Bijma J. and Elderfield H. (2016) Investigating the effects of growth rate and temperature on the B/Ca ratio and $\delta^{11}B$ during inorganic calcite formation. *Chem. Geol.* **421**, 81–92.

Kester D. R., Duedall I. W., Connors D. N. and Pytkowicz R. M. (1967) Preparation of artificial seawater. *Limnol. Oceanogr.* **12**, 176–179.

Kim S.-T., Gebbinck C. K., Mucci A. and Coplen T. B. (2014) Oxygen isotope systematics in the aragonite–CO_2–H_2O–NaCl system up to 0.7 mol/kg ionic strength at 25 °C. *Geochim. Cosmochim. Acta* **137**, 147–158.

Kim S.-T., Hillaire-Marcel C. and Mucci A. (2006) Mechanisms of equilibrium and kinetic oxygen isotope effects in synthetic aragonite at 25 °C. *Geochim. Cosmochim. Acta* **70**, 5790–5801.

Kim S.-T. and O'Neil J. R. (1997) Equilibrium and nonequilibrium oxygen isotope effects in synthetic carbonates. *Geochim. Cosmochim. Acta* **61**, 3461–3475.

Kitano Y., Okumura M. and Idogaki M. (1975) Incorporation of sodium, chloride and sulfate with calcium carbonate. *Geochem. J.* **9**, 75–84.

Kitano Y., Okumura Y. M. and Idogaki M. (1978) Coprecipitation of borate-boron with calcium carbonate. *Geochem. J.* **12**, 183–189.

Klochko K., Cody G. D., Tossell J. A., Dera P. and Kaufman A. J. (2009) Re-evaluating boron speciation in biogenic calcite and aragonite using ^{11}B MAS NMR. *Geochim. Cosmochim. Acta* **73**, 1890–1900.

Klochko K., Kaufman A. J., Yao W., Byrne R. H. and Tossell J. A. (2006) Experimental measurement of boron isotope fractionation in seawater. *Earth Planet. Sci. Lett.* **248**, 276–285.

Lambert D. K. (1996) Vibrational Stark effect of adsorbates at electrochemical interfaces. *Electrochim. Acta* **41**, 623–630.

Liu R. Y. (1988) Bootstrap procedures under some non-IID models. *Ann. Stat.* **16**, 1696–1708.

Mammen E. (1993) Bootstrap and Wild Bootstrap for High Dimensional Linear Models. *Ann. Stat.* **21**, 255–285.

Martínez-Botí M. A., Foster G. L., Chalk T. B., Rohling E. J., Sexton P. F., Lunt D. J., Pancost R. D., Badger M. P. S. and Schmidt D. N. (2015) Plio-Pleistocene climate sensitivity evaluated using high-resolution CO_2 records. *Nature* **518**, 49–54.

Mavromatis V., Gautier Q., Bosc O. and Schott J. (2013) Kinetics of Mg partition and Mg stable isotope fractionation during its incorporation in calcite. *Geochim. Cosmochim. Acta* **114**, 188–203.

Mavromatis V., Montouillout V., Noireaux J., Gaillardet J. and Schott J. (2015) Characterization of boron incorporation and speciation in calcite and aragonite from co-precipitation experiments under controlled pH, temperature and precipitation rate. *Geochim. Cosmochim. Acta* **150**, 299–313.

McCulloch M., Falter J., Trotter J. and Montagna P. (2012) Coral resilience to ocean acidification and global warming through pH up-regulation. *Nat. Clim. Change* **2**, 623–627.

McCulloch M. T., D'Olivo J. P., Falter J., Georgiou L., Holcomb M., Montagna P. and Trotter J. A. (2018) Boron Isotopic Systematics in Scleractinian Corals and the Role of pH Up-regulation. In *Boron Isotopes* (eds. H. Marschall and G. Foster). Advances in Isotope Geochemistry. Springer International Publishing, Cham. pp. 145–162. Available at: http://link.springer.com/10.1007/978-3-319-64666-4_6 [Accessed April 24, 2020].

Millero F. J. and Pierrot D. (1998) A Chemical Equilibrium Model for Natural Waters. *Aquat. Geochem.* **4**, 153–199.

Morse J. W., Arvidson R. S. and Lüttge A. (2007) Calcium Carbonate Formation and Dissolution. *Chem. Rev.* **107**, 342–381.

Moulin P. and Roques H. (2003) Zeta potential measurement of calcium carbonate. *J. Colloid Interface Sci.* **261**, 115–126.

Mucci A. (1988) Manganese uptake during calcite precipitation from seawater: Conditions leading to the formation of a pseudokutnahorite. *Geochim. Cosmochim. Acta* **52**, 1859–1868.

Mucci A. and Morse J. W. (1983) The incorporation of Mg^{2+} and Sr^{2+} into calcite overgrowths: influences of growth rate and solution composition. *Geochim. Cosmochim. Acta* **47**, 217–233.

Nehrke G., Reichart G. J., Van Cappellen P., Meile C. and Bijma J. (2007) Dependence of calcite growth rate and Sr partitioning on solution stoichiometry: Non-Kossel crystal growth. *Geochim. Cosmochim. Acta* **71**, 2240–2249.

Nielsen M. R., Sand K. K., Rodriguez-Blanco J. D., Bovet N., Generosi J., Dalby K. N. and Stipp S. L. S. (2016) Inhibition of Calcite Growth: Combined Effects of Mg^{2+} and SO_4^{2-}. *Cryst. Growth Des.* **16**, 6199–6207.

Nir O., Marvin E. and Lahav O. (2014) Accurate and self-consistent procedure for determining pH in seawater desalination brines and its manifestation in reverse osmosis modeling. *Water Res.* **64**, 187–195.

Nir O., Vengosh A., Harkness J. S., Dwyer G. S. and Lahav O. (2015) Direct measurement of the boron isotope fractionation factor: Reducing the uncertainty in reconstructing ocean paleo-pH. *Earth Planet. Sci. Lett.* **414**, 1–5.

Noireaux J., Mavromatis V., Gaillardet J., Schott J., Montouillout V., Louvat P., Rollion-Bard C. and Neuville D. R. (2015) Crystallographic control on the boron isotope paleo-pH proxy. *Earth Planet. Sci. Lett.* **430**, 398–407.

Okai T., Suzuki A., Kawahata H., Terashima S. and Imai N. (2002) Preparation of a New Geological Survey of Japan Geochemical Reference Material: Coral JCp-1. *Geostand. Newsl.* **26**, 95–99.

Owen B. B. and King E. J. (1943) The Effect of Sodium Chloride upon the Ionization of Boric Acid at Various Temperatures. *J. Am. Chem. Soc.* **65**, 1612–1620.

Parkhurst D. L. and Appelo C. A. J. (2013) *Description of input and examples for PHREEQC version 3: a computer program for speciation, batch-reaction, one-dimensional transport, and inverse geochemical calculations.*, US Geological Society. Available at: http://pubs.usgs.gov/tm/06/a43.

Penman D. E., Hönisch B., Zeebe R. E., Thomas E. and Zachos J. C. (2014) Rapid and sustained surface ocean acidification

during the Paleocene-Eocene Thermal Maximum. *Paleoceanography* **2014PA002621**.

Rae J. W. B. (2018) Boron Isotopes in Foraminifera: Systematics, Biomineralisation, and CO2 Reconstruction. In *Boron Isotopes* (eds. H. Marschall and G. Foster). Advances in Isotope Geochemistry. Springer International Publishing, Cham. pp. 107–143. Available at: http://link.springer.com/10.1007/978-3-319-64666-4_5 [Accessed March 30, 2020].

Ruiz-Agudo E., Putnis C. V., Kowacz M., Ortega-Huertas M. and Putnis A. (2012) Boron incorporation into calcite during growth: Implications for the use of boron in carbonates as a pH proxy. *Earth Planet. Sci. Lett.* **345–348**, 9–17.

Saldi G. D., Noireaux J., Louvat P., Faure L., Balan E., Schott J. and Gaillardet J. (2018) Boron isotopic fractionation during adsorption by calcite – Implication for the seawater pH proxy. *Geochim. Cosmochim. Acta* **240**, 255–273.

Sanyal A., Nugent M., Reeder R. J. and Bijma J. (2000) Seawater pH control on the boron isotopic composition of calcite: evidence from inorganic calcite precipitation experiments. *Geochim. Cosmochim. Acta* **64**, 1551–1555.

Schindler P. W. and Stumm W. (1987) The surface chemistry of oxides, hydroxides, and oxide minerals. In *Aquatic Surface Chemistry: Chemical Processes at the Particle-Water Interface* (ed. W. Stumm). John Wiley & Sons, New York, pp. 83–110.

Schoepf V., Jury C. P., Toonen R. J. and McCulloch M. T. (2017) Coral calcification mechanisms facilitate adaptive responses to ocean acidification. *Proc. R. Soc. B Biol. Sci.* **284**, 20172117.

SciPy 1.0 Contributors, Virtanen P., Gommers R., Oliphant T. E., Haberland M., Reddy T., Cournapeau D., Burovski E., Peterson P., Weckesser W., Bright J., van der Walt S. J., Brett M., Wilson J., Millman K. J., Mayorov N., Nelson A. R. J., Jones E., Kern R., Larson E., Carey C. J., Polat İ., Feng Y., Moore E. W., VanderPlas J., Laxalde D., Perktold J., Cimrman R., Henriksen I., Quintero E. A., Harris C. R., Archibald A. M., Ribeiro A. H., Pedregosa F. and van Mulbregt P. (2020) SciPy 1.0: fundamental algorithms for scientific computing in Python. *Nat. Methods* **17**, 261–272.

Sen S., Stebbins J. F., Hemming N. G. and Ghosh B. (1994) Coordination environments of B impurities in calcite and aragonite polymorphs; A ^{11}B MAS NMR study. *Am. Mineral.* **79**, 819–825.

Siffert D. and Fimbel P. (1984) Parameters affecting the sign and magnitude of the eletrokinetic potential of calcite. *Colloids Surf.* **11**, 377–389.

Smallwood P. V. (1977) Some aspects of the surface chemistry of calcite and aragonite Part I: An electrokinetic study. *Colloid Polym. Sci.* **255**, 881–886.

Stipp S. L. S. (1999) Toward a conceptual model of the calcite surface: hydration, hydrolysis, and surface potential. *Geochim. Cosmochim. Acta* **63**, 3121–3131.

Uchikawa J., Harper D. T., Penman D. E., Zachos J. C. and Zeebe R. E. (2017) Influence of solution chemistry on the boron content in inorganic calcite grown in artificial seawater. *Geochim. Cosmochim. Acta* **218**, 291–307.

Uchikawa J., Penman D. E., Zachos J. C. and Zeebe R. E. (2015) Experimental evidence for kinetic effects on B/Ca in synthetic calcite: Implications for potential $B(OH)_4^-$ and $B(OH)_3$ incorporation. *Geochim. Cosmochim. Acta* **150**, 171–191.

Vdović N. (2001) Electrokinetic behaviour of calcite — the relationship with other calcite properties. *Chem. Geol.* **177**, 241–248.

Venn A. A., Tambutte E., Holcomb M., Laurent J., Allemand D. and Tambutte S. (2013) Impact of seawater acidification on pH at the tissue-skeleton interface and calcification in reef corals. *Proc. Natl. Acad. Sci.* **110**, 1634–1639.

Wang Y.-J., Wei H.-Z., Jiang S.-Y., van de Ven T. G. M., Ling B.-P., Li Y.-C., Lin Y.-B. and Guo Q. (2018) Mechanism of boron incorporation into calcites and associated isotope fractionation in a steady-state carbonate-seawater system. *Appl. Geochem.* **98**, 221–236.

Watson E. B. (2004) A conceptual model for near-surface kinetic controls on the trace-element and stable isotope composition of abiogenic calcite crystals. *Geochim. Cosmochim. Acta* **68**, 1473–1488.

van der Weijden C. H. and van der Weijden R. D. (2014) Calcite growth: Rate dependence on saturation, on ratios of dissolved calcium and (bi)carbonate and on their complexes. *J. Cryst. Growth* **394**, 137–144.

Wolthers M., Charlet L. and Van Cappellen P. (2008) The surface chemistry of divalent metal carbonate minerals; a critical assessment of surface charge and potential data using the charge distribution multi-site ion complexation model. *Am. J. Sci.* **308**, 905–941.

Yoshimura T., Tamenori Y., Suzuki A., Kawahata H., Iwasaki N., Hasegawa H., Nguyen L. T., Kuroyanagi A., Yamazaki T., Kuroda J. and Ohkouchi N. (2017) Altervalent substitution of sodium for calcium in biogenic calcite and aragonite. *Geochim. Cosmochim. Acta* **202**, 21–38.

Yu J., Day J., Greaves M. and Elderfield H. (2005) Determination of multiple element/calcium ratios in foraminiferal calcite by quadrupole ICP-MS. *Geochem. Geophys. Geosystems* **6**, Q08P01.

Zeebe R. E., Sanyal A., Ortiz J. D. and Wolf-Gladrow D. (2001) A theoretical study of the kinetics of the boric acid–borate equilibrium in seawater. *Mar. Chem.* **73**, 113–124.

Zeebe R. E. and Wolf-Gladrow D. A. (2001) *CO_2 in seawater: Equilibrium, Kinetics, Isotopes*, Elsevier, Amsterdam.

Zhang J. and Nancollas G. H. (1998) Kink Density and Rate of Step Movement during Growth and Dissolution of an AB Crystal in a Nonstoichiometric Solution. *J. Colloid Interface Sci.* **200**, 131–145.

Associate editor: Mariette Wolther